Alma Mater Studiorum · Università di Bologna

Scuola di Scienze

Dipartimento di Fisica e Astronomia

Corso di Laurea Magistrale in Fisica

Study of neutron transmission on ^{154,155,157}Gd at neutron time-of-flight facility GELINA

Relatore:

Dott. Cristian Massimi

Presentata da:

Riccardo Mucciola

Correlatori:

Dott. Carlos Paradela

Prof. Gianni Vannini

Anno Accademico 2018/2019

Abstract

In questa tesi verrà discussa la misura della trasmissione sugli isotopi ^{154,155,155}Gd per energie inferiori ai 100 eV. La finalità principale di questo studio è quella di ridurre l'incertezza sulla sezione d'urto di cattura neutronica, la quale è necessaria per le tecnologie nucleari, per la medicina nucleare e per lo sviluppo di rivelatori per neutrini. In particolare, ho analizzato le misure di trasmissione effettuate presso la facility di tempo di volo GELINA, EC-JRC-Geel (Belgio). Le misure sono state effettuate con condizioni di fascio differenti e sono stati utilizzati 9 diversi campioni al fine di ridurre l'incertezza sistematica legata al campione stesso. I campioni utilizzati sono: cinque dischi metallici arrichiti in ^{154,155,157}Gd precedentemente utilizzati in una campagna di misura ad n_TOF e quattro leghe di magnesio con il 0.25% wt di gadolinio naturale. La trasmissione è stata misurata presso la sala sperimentale posta a 10 m dalla sorgente di neutroni. La data reduction è stata effettuata utilizzando un sowtware specifico. Le sezioni d'urto ottenute da questa analisi verranno inviate al database open-access EXFOR.

Abstract

The measurements of transmission on ^{154,155,157}Gd for energies below 100 eV are discussed in this thesis. This study aimed at reducing the uncertainty to provide very accurate cross section data relevant for nuclear technology, nuclear medicine and detector development. In particular, I have analysed the transmission measurements carried out at the neutron time-of-flight facility GELINA at the EC-JRC-Geel (Belgium). The measurements were performed under different neutron irradiation conditions, using 9 different samples in order to minimize systematic uncertainties related to the samples, which was the main limitation in previous experiments. The samples analysed in this work are five isotopically enriched ^{154,155,157}Gd metallic disks used in a previous capture measurement at the n_TOF facility at CERN and four samples consisting in an alloy of magnesium with a 0.25%wt of ^{nat}Gd. Transmission experiments were carried at a measurement station located at 10 m from the neutron source. I have performed the data reduction of these transmission measurements using dedicated software programs. The resulting cross sections data for ^{154,155,157}Gd will be delivered to the publicly available experimental nuclear reaction database EXFOR.

Contents

Introduction

One of the key characteristics of neutron-induced reactions with nuclei is the resonance structure at very low kinetic energies. Since the neutron is electrically neutral, it does not suffer from Coulomb repulsion and it has negligible interaction with electrons. Therefore, neutrons can interact directly with the atomic nucleus even at very low kinetic energies ($\approx$ meV). In the low energy region, the neutron cross section can change many orders of magnitude in a very small energy region. The resonances are caused by the excitation of nuclear energy levels on the compound nucleus formed by the neutron and the original nucleus. The excitation energy of these levels is usually in the MeV region (5-10 MeV).

Typically the measured width Γ of these resonances is in the meV region. Therefore, according to Heisenberg's uncertainty principle, the mean life time of a compound nucleus is $t = \hbar/\Gamma \approx 10^{-15}$ s, which is several orders of magnitude larger than the time needed by a neutron to cross a nucleus without interacting with it. The compound nucleus will then decay in one of the allowed channels. The mode of decay and the decay probability are considered independent from the way the compound nucleus was created. The decay probability in each channel is given by the branching ratio, which is defined as the ratio of the width related to a particular channel Γ_x (e.g. Γ_γ, Γ_n...) with the total width Γ. For low energy neutrons, the available channels are γ decay (radiative capture), neutron emission (elastic scattering) or fission.

Neutron-induced reaction are fundamental in many scientific fields. First of all, they are crucial in reactor physics for safety and risk-related evaluations (burnable neutron poisons, control rods, etc.). Moreover, an accurate knowledge of the cross sections of reactions on specific isotopes is important to improve the efficiency of nuclear power

plants. Furthermore, the development of new generation systems like ADS (Accelerator Driven System) or high-density research cores relies on complete and accurate neutron reaction data. Neutron-induced reaction plays a fundamental role in many other scientific fields, ranging from nuclear medicine to astrophysics. In nuclear medicine, many new anti-tumoral techniques are under development (e.g. Boron Neutron Capture Therapy). The use of neutrons in medicine can help to reduce the amount of radiation absorbed by the patient during the treatment. Also, the knowledge of the cross sections of neutron-nucleus reactions is necessary for a better comprehension of nuclear astrophysics. They can be used to test stellar evolution models since the production of heavy elements is caused by subsequent neutron captures inside stars. Furthermore, a precise knowledge of the neutron cross section can help to develop new and more efficient neutrino detectors. Gadolinium is important in all these fields. A review of all the main application of gadolinium in these fields is performed in Chapter 1.

Although gadolinium neutron cross section is necessary for many fields, the data in literature are not compatible with each other. The main libraries for nuclear data are ENDF/B-VIII, JEFF-3.3, and JENDL-4.0 which are respectively the United States, Europe, and Japan nuclear data library. The data in these libraries are not compatible with some of the latest measurement of the gadolinium capture cross section at thermal energies. In particular, we have deviations up to 12% for ^{157}Gd and up to 7% for ^{155}Gd. A more accurate description of the data in the literature is performed in Chapter 2. In order to reduce the uncertainties on these cross sections a new and more accurate evaluation of the neutron capture cross section of both ^{155,157}Gd is necessary. With this aim transmission measurements were performed at the time-of-flight facility GELINA, located in the JRC of Geel. The measurement was performed using enriched and natural samples. In particular, the same enriched samples were used in a previous experimental campaign at n_TOF for a radiative capture measurement [1]. An overview of the experimental facility and the samples used in this experiment are presented in Chapter 3.

The data reduction procedure was performed using the AGS code developed at JRC.

Using this code it was possible to obtain transmission spectra corrected by the estimated background. Using the R-Matrix code REFIT [2] the spectra were corrected for other experimental effects such as the resolution function and the Doppler broadening. All the data reduction procedure is presented in Chapter 4. All the results obtained in these measurements, ranging from total cross section to resonance parameters are presented in Chapter 5.

Chapter 1

Scientific motivations

Gadolinium is one of the nuclides with the highest neutron capture cross section, mainly thanks to the odd isotopes ^{155}Gd and ^{157}Gd. These isotopes have respectively a thermal capture cross section of about 60 kb and 250 kb. This huge cross section makes gadolinium a fundamental nuclide in many scientific fields ranging from nuclear power plant safety to nuclear medicine. Despite its importance, its thermal cross section is not known with good precision. All these factors made necessary a new measurement of the total cross section on gadolinium isotopes. A transmission experiment using ^{154,155,157}Gd enriched samples and Mg 0.25% wt ^{nat}Gd alloys was proposed to EUFRAT [3] (European facility for nuclear reaction and decay data measurements) and it was carried out using the GELINA facility located in the JRC of Geel, Belgium.

1.1 Nuclear power plants

One of the main application fields of gadolinium is nuclear energy production. In fact, gadolinium is often used as a "burnable neutron poison" in 2nd and 3rd generation light-water reactors. These poisons must have a thermal cross section much higher of the fission cross section of ^{235}U to compete with the fission reaction inside the reactor core. These poisons allow loading the core with higher enriched uranium safely compensating for the higher initial neutron flux. During the operation of the reactor, both poison and

^{235}U are burnt so that the effect of the poison becomes less and less important until the poison completely disappears at a point in the cycle of the fuel at which the remaining amount of fissile material can be easily controlled. In this way is possible to increase the overall length of the fuel cycle by allowing higher amounts of fissile materials loaded in Fuel Assemblies (FAs) and then in reactor cores. This will increase the efficiency of the power plant. In fact, the use of neutron poisons allows the operator to reload fuel into cores less often and after a longer period of uninterrupted operation. One of the most common neutron poison is gadolinia (Gd_2O_3) that is mixed directly within the UO_2 fuel matrix. This ensures that the burnable neutron poison is never separated from the active material and this will also enhance the mechanical properties of the fuel [4].

Gadolinium was used for the first time in a commercial reactor in 1973. Nowadays it is used in the Cyclades and Gemmes core management scheme by Electricité de France in its CP0 and 1300 MWe PWR reactors, respectively [5]. Gadolinia is not necessarily present in all FAs. The Gemmes scheme, for example, foresees a reload of 64 FAs, 24 of which are doped with Gd_2O_3. The choice of the position of the doped FAs is dictated by an optimization of the power density distribution.

As already mentioned before, the high cross section of natural gadolinium is provided by its odd isotopes ^{157}Gd and to a lesser extent ^{155}Gd. The proper knowledge of these cross sections is not only important at the beginning of the life of an FA but also during its life cycle. In fact, an accurate prediction of the burning rate of gadolinium is fundamental for predicting the appearance of the FA reactivity peak and its intensity. To verify the predicted Gd burn-up and depletion in Monte Carlo codes a series of experiments using the Melusine research reactor in Grenoble have been performed by CEA (Commissariat à l'énergie atomique et aux énergies alternatives) [6]. The most recent work on the comparison between experiment and calculation is that of 2015 by Bernard and Santamarina [7]. In this work, we can notice that, while the prediction on some gadolinium isotopes looks quite good, there are still some non-negligible differences for ^{157}Gd. This suggests a possible incorrect prediction of the capture cross section of this isotope.

A good prediction of the depletion of gadolinium inside the reactor core is necessary to estimate the so-called "residual reactivity penalty". This is essentially the value of anti-reactivity associated to the high burn-up. The residual reactivity penalty is important because, if too high, it can limit the time a given FA can be used at full power. To give an example of this effect the reactivity penalty due to 16 gadolinium fuel pins with initial 8.0% wt of gadolinia in UO_2 for a 17×17 PWR FA (4.5% wt ^{235}U) correspond to the loss of 5 full power days per year [8]. In the energetic market of France, this corresponds to a loss of 8M€[9]. Although burnable neutron poisons such as gadolinium are not used in natural uranium Canadian Deuterium Uranium (CANDU) reactors they can be used for enriched fueled heavy water reactors. In fact, using a neutron poison inside a fissile enriched CANDU can help in several ways:

1. reduce void effects;
2. maximize fissile content of fresh fuel
3. suppress initial reactivity excess
4. control the power shape

The advantages of using neutron poisons inside a CANDU reactor fueled with enriched MOX were proved by Serghiuta and Nainer [10].

Another important role of gadolinium inside nuclear power plants is the contribution to the uncertainty in the multiplication factor k. The multiplication factor is defined as the ratio of the number of neutrons in one generation to the number in the preceding generation. In Tab1.1 the first contribution, in decreasing importance, to the uncertainty of k are shown.

These data are relative to the General Electric 10×10-8 BWR reactor at a moderator density of 0.45 g/cm^3. The rank in the table is defined as the contribution to the uncertainty divided by the reference value which is the contribution of ^{235}U. As we can see the capture reaction in $^{155,157}Gd$ represents the main contribution to uncertainty after

uranium. As a consequence, any improvement in the ^{157}Gd(n,γ) cross-section in the low energy range can have a significant impact on the overall assessment of the neutronic properties of nuclear reactors using gadolinium as a neutron poison.

Reaction/Nuclide	Contribution to Uncertainty ($\%\Delta k/k$)	Rank
^{235}U$\bar{\nu}$	0.270	1.00
^{238}U(n,γ)	0.197	0.81
^{235}U(n,γ)	0.143	0.64
^{235}U(n,f)	0.143	0.56
^{238}U(n,n')	0.120	0.51
^{238}U $\bar{\nu}$	0.0711	0.32
^{157}Gd(n,γ)	0.0603	0.26
^{155}Gd(n,γ)	0.0448	0.20
^{92}Zr(n,γ)	0.0429	0.16
^{1}H(n,γ)	0.0367	0.14
^{91}Zr(n,γ)	0.0348	0.13

Table 1.1: Main contribution to k uncertainty in a GE 10×10-8 reactor

1.2 Neutrino Detector

In the last years, gadolinium became very important also for neutrino detectors. In fact the presence of gadolinium inside a detector enhances the tagging of neutrons produced from the inverse beta decay (IBD) reaction of the MeV $\bar{\nu}_e$ on a free proton: $\bar{\nu}_e + p \rightarrow n + e^+$.

To accurately detect a $\bar{\nu}_e$ a coincidence of a prompt signal with a delayed one is necessary. The prompt signal occurs a few nanoseconds after the interaction and originates from the annihilation of the emitted positron. The delayed signal is generated from the γ

emission following the capture of the thermalized neutrons. Neutrons produced by IBD in the MeV region usually have energies up to several tens of keV and need to interact at least ten or twenty times with hydrogen before being thermalized. For water Cherenkov detectors the mean neutron capture time is usually on the order of a few tens of microseconds. To enhance the neutron capture cross section of the detector it has become common to add a mass fraction of 0.1%-0.2% of gadolinium into the neutrino targets of organic liquid scintillators and water Cherenkov detectors [11]. The demonstrated feasibility to load common neutrino target materials with gadolinium is based not only on the high cross section but also in the high Q-value of the capture reaction. In fact, we have that the Q value for neutron capture in ^{157}Gd is 7.9 MeV. This energy is released in several γ rays.

One of the main neutrino detectors that are using Gd-doped target is Super Kamiokande (SK) [12], the water Cherenkov detector built-in Kamioka (Japan). The upgrade of the detector started in 2018 and the data taking started in January of 2019. The effect of gadolinium inside SK was tested in the EGADS facility, built in the mines near the detector, no signs of rust or deterioration was apparent with a concentration of $Gd_2(SO_4)$ up to 0.2%. The same concentration of gadolinium salt was used for SK. As a result, 100 tons of $Gd_2(SO_4)$ were added to the SK ultra-pure water. To reach a contaminant level below the requirements a high-purity salt was used [13].

1.3 Boron Neutron Capture Therapy

Another important application field for gadolinium is the nuclear treatment of cancer, in particular, the Boron Neutron Capture Therapy (BNCT). BNCT is an experimental binary radiation therapy currently under intense scrutiny for the treatment of cancer. The neutron capture on ^{10}B causes the creation of the unstable isotope ^{11}B that decay emitting highly ionizing ^{7}Li and α particle. These particles release energy in a very short range in the human cells, usually below 10 μm. Thus is possible to kill tumour cells without affecting adjacent healthy cells if the boron is correctly accumulated in the

intracellular space. It has been estimated that around 30 μg of boron are needed per gram of tumour in order to achieve a good therapeutic advantage in reasonable irradiation time. To obtain a good concentration in the tumour cell keeping at the same time a low concentration in the surrounding healthy cells selective delivery drugs are necessary. To monitor the concentration of boron in the tumour cells imaging techniques are needed. The possible imaging techniques are Positron Emission Tomography (PET) or Magnetic Resonance Imaging (MRI). PET is more sensitive but requires the administration of further reactivity (e.g. ^{18}F) while MRI appears the best option. In fact, the high spatial resolution of about 100 μm provides detailed functional information without using a radioactive nuclide.

The possibility to use gadolinium doped ligands together with boron was tested at the University of Pavia (Italy). The experiment was carried out at the TRIGA Mark II reactor on three groups of mice using the ^{10}B enriched AT101 ligand. The ligand was chelated using $GdCl_3$ enriched in ^{157}Gd. In this way is possible to achieve 65 times improvement upon the ^{10}B capture. The emitted γ rays following the neutron capture on gadolinium have a very short range, between 0.5 nm and 1.4 μm. Moreover, the presence of Gd can be used to measure indirectly the concentration of boron in tumour cells using MRI. For irradiated and treated mice no growth of tumour size was detected in the first 25 days after BNCT [14].

Chapter 2

Data in literature

In the last 50 years a number of measurements of the ^{155,157}Gd thermal cross sections were performed but not all the results are compatible with each other. The cross section spectra are available in nuclear data libraries as ENDF/B-VIII.0, JEFF-3.3 and JENDL-4.0. In particular, ENDF/B-VIII.0 is based on the resonance parameters of the Brookhaven National Laboratory compilation (BNL-325) by Mughabghab [15]. JEFF-3.3 uses data from previous libraries: for ^{155}Gd it uses data present in JEF-2.2 which is based on Möller measurement [16] while for ^{157}Gd it uses data from JENDL-3.2 which is based on the evaluation taken from BNL-325(3rd edition) [17]. In JENDL-4.0 the resonance parameters are based on the Leinweber experiment [18]. A brief review of some of the previous measurements of transmission and capture on ^{155,157}Gd is reported in the following section. A comparison of the thermal cross sections obtained by those experiments with data in libraries will be performed.

2.1 Experiments overview

In the past years, different measurements of the ^{155,157}Gd thermal cross section were performed using different techniques. In fact, the two major techniques used for neutron-induced reaction cross section are time-of-flight and reactor measurements. The first one allows to have a pulsed beam and a wide and adjustable energy range while for fission

reactors we have a continuous neutron flux with a fixed energy spectrum. The most used technique is the time-of-flight one which was used by several scientists: Möller and collaborator at the Brookhaven National Laboratory [16], Leinweber [18], and Kang [19] at Rensselaer Polytechnic Facility, Baramsai and collaborators at the Los Alamos Neutron Science Center [20] and Mastromarco and collaborators at n_TOF [1]. A cross section measurement at a fission reactor was performed by Choi and collaborators at the Budapest Research Reactor [21]. Another very important measurement performed using a reactor is the one of Ohno and collaborators at the JRR-2 reactor in Japan [22].

For all these measurements the thermal capture cross section for the odd isotopes of gadolinium was obtained using the resonance parameters of the low-energy resonance of these isotopes. All the time-of-flight measurements were performed using liquid or metallic enriched samples, while the Choi measurement was performed using a natural sample. A brief description of all these measurements is performed in the following.

2.1.1 Transmission measurement at BNL by Möller

One of the oldest measurements of the gadolinium capture cross section for thermal neutrons is the one by Möller and collaborators [16]. This measurement was carried out at the Brookhaven National Laboratory (USA) in 1960. They performed a transmission measurement using a crystal spectrometer. A Bragg reflection can occur only if $n\lambda = 2d_{jkl}\sin\theta_{jkl}$ where λ is the neutron wavelength, d_{jkl} is the distance between two crystal planes and θ_{jkl} is the angle of incidence of the neutron with that plane. Measuring the incident angle is possible to obtain a monochromatic reflected beam. The energy resolution depends on four factors: the precision of the measurement of the Bragg angle, knowledge of the crystal lattice, identification of crystal planes giving the reflection and precision of construction and adjustment of the spectrometer. Using a particular Be crystalline plane a neutron energy resolution ($\Delta E/E$) of 3.4×10^{-3} and 1.2×10^{-2} was obtained at 0.5 eV and 0.02 eV respectively. Möller and collaborators measured the cross section of five different samples of gadolinium: ^{nat}Gd, ^{155}Gd, ^{156}Gd, ^{157}Gd and ^{158}Gd. All the samples were prepared as a heavy water solution of the nitrates starting with the

isotopically enriched oxide Gd_2O. The enrichment are shown in Tab.2.1.

Sample	^{155}Gd (%)	^{156}Gd (%)	^{157}Gd (%)	^{158}Gd (%)
^{nat}Gd	14.78	20.59	15.71	24.78
^{155}Gd	74.1(1)	17.8(1)	3.84(5)	2.61(5)
^{156}Gd	4.34(3)	80.22(8)	10.02(4)	4.30(4)
^{157}Gd	1.34(5)	7.30(5)	69.6(1)	19.5(1)
^{158}Gd	0.30(2)	0.84(3)	3.15(5)	92.87(11)

Table 2.1: Enrichment of the gadolinium samples used in the Möller experiment.

The solutions were sealed into precision cells made of fuse quartz. Tests with a neutron spectrometer were made to ensure that the quartz cells were identical within 0.2% in physical thickness and neutron transmission. The concentration of the samples was known to better than 0.5%. The transmission measurements were done with respect to a cell filled with D_2O called "dummy sample". Because the "dummy sample" contained only heavy water while the samples had NO_3 it was necessary to apply some calculated correction. The correction was smaller then 1%. Möller corrected the results for the instrument resolution, Doppler broadening and the superimposition of different resonances at similar energies for different isotopes (^{155}Gd and ^{157}Gd). The instrument resolution correction amounts only 0.45% for the resonance region. For the Doppler broadening Möller shows that for low energy neutrons the Doppler width Δ is proportional to $E^{1/2}$ where E is the neutron energy. For high energy resonances, Δ is approximately constant and it is proportional to $E_0^{1/2}$ where E_0 is the resonance energy. For the thermal resonances of gadolinium, the Doppler broadening correction is smaller than 0.2%. To derive the individual cross section of ^{155}Gd and ^{157}Gd three samples with different enrichments of gadolinium where used. The enrichments used for this measurement are not reported in the article. Several low energy resonances were identified between 0.2 and 24 eV, in Table 2.2 the resonance parameter for the first 2 resonances of ^{155}Gd and ^{157}Gd.

The resulting thermal capture cross sections are $\sigma^{155} = 60600 \pm 500$ barns and $\sigma^{157} = 254000 \pm 2000$ barns.

	^{155}Gd	^{157}Gd
E_0 (eV)	0.0268(2)	0.0314(2)
Γ (eV)	0.108(1)	0.107(1)
Γ_γ(eV)	0.108(1)	0.106(1)
$2g\Gamma_n$(meV)	0.130(2)	0.590(10)
σ^{th} (kb)	58.9(5)	230(2)

Table 2.2: Resonance parameters for the first two resonances of ^{155}Gd and ^{157}Gd obtained by Möller.

2.1.2 Transmission measurement at JRR-2 by Ohno

A very important measurement of gadolinium thermal cross section was performed by Ohno and collaborators [22]. However the original article is no longer available, some of the main characteristics of the experiment can be found in the EXFOR database [23].

The transmission measurement was performed in 1968 using a neutron beam produced by the JRR-2 (Japanese Research Reactor No.2), a heavy water moderated reactor which worked with enriched uranium (45%). The samples used in this experiment were liquid enriched samples made of gadolinium oxide diluted in DNO_3D_2O solution. The neutrons were detected using a crystal spectrometer made of LiF. Ohno and collaborators measured the thermal cross section of both ^{155,157}Gd. The obtained cross sections are shown in Tab.2.3.

	^{155}Gd	^{157}Gd
σ (kb)	61.9(6)	248(4)

Table 2.3: Thermal cross section of ^{155,157}Gd obtained by Ohno and collaborators.

2.1.3 Transmission and capture measurement at RPI by Leinweber

Another important measurement of the thermal cross section of gadolinium was performed by Leinweber and collaborators [18]. This measurement was carried out at the Rensselaer Polytechnic Institute (USA) LINAC facility in 2006. Leinweber and collaborators measured capture and total cross section with the time-of-flight technique. The measure was carried out at a 25 m flight-path station. Nine liquid samples (four ^{155}Gd enriched and five ^{157}Gd enriched) and ten metal samples (^{nat}Gd) were used. The enrichment of the samples is shown in Tab 2.4.

Sample	^{152}Gd (%)	^{154}Gd (%)	^{155}Gd (%)	^{156}Gd (%)	^{157}Gd (%)	^{158}Gd (%)	^{160}Gd (%)
^{155}Gd	0.0108(2)	0.9859(74)	74.4233(95)	17.5674(51)	3.7513(23)	2.5336(24)	0.7278(20)
^{157}Gd	0.00510(4)	0.07530(25)	1.35147(70)	7.3627(17)	69.6623(81)	19.4431(67)	2.1000(15)

Table 2.4: Enrichment of the gadolinium samples used in the Leinweber experiment.

The liquid samples were prepared by dissolving gadolinium oxide into D_2NO_3 and then diluting in 99.80% pure D_2O. All the liquid samples were enclosed in quartz cells. All metal samples were sealed inside aluminium sample cans.

The transmission detectors were: a 0.3 cm thick NE 905 ^{6}Li scintillator covering the energy range from 0.002 to 10 eV and a 1.27 cm thick NE 905 ^{6}Li scintillator covering the energy range from 1 to 300 eV. The capture detector was a 20 litre NaI(Tl) scintillator divided into 16 optically isolated segments forming an annulus around the neutron beam with the sample at its centre. The neutron flux was measured mounting a thick $^{10}B_4C$ sample in the beam and adjusting the total energy threshold to record the 478 keV γ ray from neutron capture in boron.

For transmission, a measurement using a dummy sample containing pure D_2O was carried out, in this way the effect of quartz and heavy water cancel out in the ratio for liquid samples. For capture, measurements with a liquid sample containing pure heavy water and with an empty aluminium sample were performed. The thermal yield was

normalized to the transmission data using a combined SAMMY fit while the epithermal yield was normalized to the black 6.3 eV resonance of gadolinium. The resonance parameters were extracted from the data using the SAMMY R-Matrix code. The parameters for the first resonances of ^{155}Gd and ^{157}Gd are shown in Table 2.5. The thermal cross sections obtained by Leinweber were 60.2 kb and 226 kb for ^{155}Gd and ^{157}Gd respectively. No cross section uncertainty was explicitly reported in the original article.

	^{155}Gd	^{157}Gd
E_0 (eV)	0.025 ± 0.003	0.032 ± 0.003
Γ_γ(meV)	104 ± 3	107 ± 3
Γ_n (meV)	0.097 ± 0.003	0.428 ± 0.004

Table 2.5: Resonance parameter for the first two resonance of ^{155}Gd and ^{157}Gd obtained by Leinweber.

Leinweber also measured the resonance integrals from 0.5 ev to 20 MeV. The resonance integral (RI) is defined as:

$$RI = \int_{0.5ev}^{20MeV} \sigma_c(E)\frac{dE}{E} \tag{2.1}$$

The RI measured for ^{nat}Gd was 402 b.

2.1.4 Capture measurement at RPI by Kang

Y.R. Kang and collaborators measured capture cross section of ^{155}Gd and ^{157}Gd using the time-of-flight technique. This measure was carried out at the RPI linac in 2015 [19]. The capture detector was the same as Leinweber. Kang used five isotopically enriched Gd metal samples and two ^{nat}Gd samples of different thicknesses. All the samples were sealed into aluminium sample cans. The isotopical enrichment of the samples is shown in Tab.2.6.

The influence of the aluminium cans was measured by including an empty sample can in the capture measurement. The resonance parameters were obtained from the data

Sample	^{152}Gd (%)	^{154}Gd (%)	^{155}Gd (%)	^{156}Gd (%)	^{157}Gd (%)	^{158}Gd (%)	^{160}Gd (%)
^{155}Gd	0.04	0.64(2)	91.74(10)	5.11(10)	1.12(5)	0.94(5)	0.41(2)
^{156}Gd	< 0.01	0.11(1)	1.96(2)	93.79(3)	2.53(2)	1.20(2)	0.41(2)
^{157}Gd	< 0.02	0.16(1)	0.81(2)	2.21(3)	90.96(8)	5.08(5)	0.80(2)
^{158}Gd	< 0.1	< 0.1	0.96(5)	1.70(5)	3.56(5)	92.00(10)	1.82(5)
^{160}Gd	< 0.01	0.02(0)	0.18(1)	0.32(2)	0.43(2)	0.93(2)	98.12(5)

Table 2.6: Enrichment of the gadolinium samples in the Kang experiment

using the SAMMY code. The epithermal capture resolution function was fitted to ^{238}U to enhance the precision of epithermal resonance parameters. The effects of Doppler broadening, resolution broadening and multiple scattering were added to the code. The first two resonances for ^{155}Gd and ^{157}Gd are shown in Table 2.7. The RI between 0.5 eV and 20 MeV for ^{nat}Gd was also measured. The resulting RI was 395 ± 2 b. The thermal cross sections were not reported in the article.

	^{155}Gd	^{157}Gd
E_0 (eV)	0.025 ± 0.003	0.032 ± 0.003
Γ_γ(meV)	104 ± 3	107 ± 3
$2g\Gamma_n$ (meV)	0.097 ± 0.003	0.428 ± 0.004

Table 2.7: Resonance parameter for the first two resonance of ^{155}Gd and ^{157}Gd obtained by Kang.

2.1.5 Capture measurement at LANSCE by Baramsai

In 2012 Baramsai and collaborator measured ^{155}Gd capture cross section at the Los Alamos Neutron Science Center (USA) [20]. They used the time-of-flight technique with a neutron beam with energy between 1.36 eV and 1 MeV. They used the DANCE γ-ray calorimeter array that consists of 160 BaF_2 crystals arranged in a 4π geometry. This

detector allowed Baramsai to precisely determine the time-of-flight of neutrons, discriminate events by the Q-value of the reaction, identify coincidence γ rays following capture and measure the multiplicity of the emitted photons. The samples were self-supporting metal foils enriched at 91.74% in ^{155}Gd. The enrichment and the contaminants of the samples are shown in Tab.2.8. No uncertainties are provided for the enrichments.

Sample	^{154}Gd (%)	^{155}Gd (%)	^{156}Gd (%)	^{157}Gd (%)	^{158}Gd (%)
^{155}Gd	0.63	91.74	5.12	1.14	0.94

Table 2.8: Enrichment of the gadolinium samples used in the Baramsai experiment.

The constant background was given by natural radioactivity of the detector, time-of-flight dependent background and from neutron scattered from the sample. The natural radioactivity was suppressed by the waveform analysis and by an energy threshold. With an energy threshold was also possible to reduce the background coming from neutron capture of different gadolinium isotopes. The only exception is ^{157}Gd that have a very similar Q-value with respect to ^{155}Gd. To reduce the background induced by neutrons scattered by the sample and captured by barium isotopes a ^{6}LiH shell of 6 cm surrounds the target to absorbs scattered neutrons. The remaining contribution of neutron capture from Ba was subtracted using a measurement of a ^{208}Pb sample.

The neutron flux was measured with two detectors: a proportional chamber filled with BF_3+Ar enriched in ^{10}B and a ^{6}LiF target. The yield was normalized using the 4.9 eV resonance of gold and its cross section. An estimate of the single-photon detection efficiency was carried out comparing GEANT4 simulation with experimental data from ^{60}Co, ^{88}Y and ^{22}Na. The total efficiency for a given multiplicity of photons was carried out using theoretical models of Level Distribution (LD) and Photon Strength Functions (PSF) and using the information of the model to simulate the photon cascade. The simulation showed that the fraction of detected cascade is insensitive to the spin and it reaches a value of 30.5%. The spins of the resonances were determined using a pattern recognition method (PRM). With this method, one can determine the spin of a resonance measuring the multiplicity of the emitted photons. This technique doesn't use a single

resonance as a prototype for the analysis but determines the density function based on the data. It then introduces a discriminant function based on the estimated PDF. With this method, Baramsai determined the spin for almost all the resonance up to 185 eV.

The systematic uncertainties in the determination of cross section are areal density, area of the target, neutron flux and detection efficiency. The uncertainties of areal density and area are about 0.5%, the neutron flux uncertainties were measured using the beam monitors and is about 3%, the detection efficiency uncertainties were estimated using simulation code like DICEBOX [24] and GEANT4 and are estimated to be 3%. The resonance parameters were extracted from the data using the SAMMY code.

2.1.6 Capture measurement at BPR by Choi

Another measure of ^{155}Gd and ^{157}Gd cross section was carried out by Choi and collaborators [21]. The measurement was carried out with a cold neutron beam at the Budapest Research Reactor. The detector was a Compton-suppressed spectrometer comprising a high-purity germanium detector, an annulus guard detector of bismuth germanate and a surrounding lead shield. The sample was 10 mg with natural abundance of GdB_6. To normalize the gadolinium cross section the boron capture cross section was used. The deviation from $1/v$ spectrum of the capture cross section was measured using the Westcott factor [26]. The Westcott factor is defined as the ratio of the Maxwellian averaged cross section with the thermal cross section and it allows to evaluate the non $1/v$ behaviour of the capture cross section (Westcott factor g significantly different from unity). In this experiment the Westcott factor was modified for a non-Maxwellian neutron flux and the thickness of target:

$$g^*_{eff} = \frac{1}{\sigma_0 v_0} \frac{\int_0^\infty \sigma_\gamma(\lambda) v(\lambda) n^*(\lambda) d\lambda}{\int_0^\infty n^*(\lambda) d\lambda} \tag{2.2}$$

where $n^*(\lambda) = \frac{n(\lambda)[1-e^{-N\sigma}]}{N\sigma}$ is the observed neutron spectrum $n(\lambda)$ modified by the absorption of sample, σ_0 is the thermal capture cross section, v_0 is the thermal speed of neutron and $\sigma_\gamma(\lambda)$ and $v(\lambda)$ are respectively the capture cross section and the neutron speed at wavelength λ. The g^*_{eff} calculated with the data are 0.887 for ^{155}Gd and 0.859

for ^{157}Gd. No correction for Doppler broadening is attempted since this effect was very small (0.1% of resonance area with E< 0.1 eV). The thermal cross section was extracted using the equation:

$$\sigma_0 = \sum_{i=1}^{n} \frac{\sigma_{i\gamma g}^{exp}(1+\alpha_{ig})}{(g_{eff}^{*})_{i\gamma}} + \sum_{j} \sigma_{j\gamma g}^{sim}(1+\alpha_{jg}) \tag{2.3}$$

where the first sum over i is for level below E_{crit} while the second sum over j is for level above E_{crit}. The cross section $\sigma_{i\gamma g}$ are the partial cross section of decay from state i to the ground state. The subscript *exp* denotes experimental quantities while the subscript *sim* denotes simulated ones. α_{ig} denote the internal conversion coefficients. The decay width for γ emission was calculated using theoretical models of Level Density (LD), Photon Strength Function (PSF). The total decay width of level i is given by:

$$\Gamma_{i\gamma} = \sum_{f} \frac{1}{\rho(E_i, J_i, \pi_i)} \sum_{X,L} y_{XL}^2 E_{\gamma}^{2L+1} f_{XL}(E_{\gamma}, \xi) \tag{2.4}$$

where ρ is the LD of the compound nucleus, f_{XL} is the PSF for the transition of type X (electric or magnetic) with multipolarity L and y_{XL} is a random number from a gaussian distribution that simulates the Porter-Thomas fluctuations [25]. The study aimed to find the best description of experimental data tuning the statistical models. Using the best fit models of LD and PSF obtained with the decay width is possible to estimate the second sum of Eq.2.3. In this way the thermal capture cross section obtained were: 56.7(21) kb for ^{155}Gd and 239(6) kb for ^{157}Gd.

2.1.7 Capture measurement at n_TOF by Mastromarco

The more recent measurement of ^{155}Gd and ^{157}Gd capture cross section was carried out by Mastromarco and collaborators [1] at the n_TOF facility at CERN. The capture detector was an array of four C_6D_6 liquid scintillators. These detectors have a very low sensitivity to background signals induced by sample-scattered neutrons. The scintillators were calibrated using standard γ ray sources, namely ^{137}Cs, ^{88}Y, Am-Be and Cm-C. The samples were made of self-supporting enriched gadolinium metallic discs. Two samples

of different thicknesses were used for the measurements of capture with neutron energy up to 1 keV. The main characteristics of the samples are shown in Tab2.9.

Sample	Abundance %	Contamination ^{155}Gd or ^{157}Gd	Main contaminant %	Weight mg	Areal density atoms/barns$\times 10^{-8}$
^{155}Gd	91.74(18)	1.14(1)	5.12(18) ^{156}Gd	100.6(1)	12440(40)
^{155}Gd	91.74(18)	1.14(1)	5.12(18) ^{156}Gd	10.0(1)	1236(12)
^{157}Gd	88.32(1)	0.29(1)	9.10(1) ^{158}Gd	191.6(1)	23390(60)
^{157}Gd	88.32(1)	0.29(1)	9.10(1) ^{158}Gd	4.7(1)	574(12)

Table 2.9: Characteristics of the gadolinium samples in the n_TOF experiment

A ^{197}Au and a lead sample were used for the normalization and the determination of background respectively. The relative energy resolution of the n_TOF spectrometer is of the order of 5.4×10^{-4} at 1 keV thus the energy resolution is smaller than the total width of neutron resonances up to 250 eV. The Doppler broadening starts to dominate the observed width for energies above 10 eV.

The neutron flux was measured using the silicon monitor SiMON that is based on the ^{6}Li(n,t)α reaction. This detector is almost transparent to neutrons, the absorption of this detector is less than 1.4%. The capture yield Y(E_n) was obtained from the relation:

$$Y(E_n) = \frac{N}{S_n + E_n \frac{A}{A+1}} \frac{C_w(E_n) - B_w(E_n)}{\varphi_n(E_n) f_{BIF}(E_n)} \tag{2.5}$$

were C_w is the weighted counting rate, N is a normalization factor, S_n the neutron separation energy of the compound nucleus, A the mass number, B_w the weighted background rate, φ_n the neutron fluence and f_{BIF} a correction factor taking into account the variation of the spallation profile of the neutron beam. The background (B_w) has many components: neutron beam interaction with something different from the sample, sample-scattered neutrons, γ travelling in the beam and time-independent background. The first component was evaluated with a measurement without the sample. The second one using a lead sample from which the counts of the empty sample were subtracted. The third one was mainly caused by capture of hydrogen and boron in the moderator, this

kind of background starts to contribute at energy above 300 eV and was evaluated using the lead sample. The fourth component was measured with a beam off measurements. The normalization parameter N was obtained with the saturated resonance technique [27] using the 4.9 eV resonance of gold. The f_{BIF} factor was measured with a technique similar to the saturated resonance. Using the thick gadolinium sample the expected capture yield is 1 for neutron energy below 1 eV, any departure from this behaviour can be ascribed to a variation of the beam interception factor.

The capture yield was analysed using the code SAMMY. The resonance above 307 eV and 181 eV respectively for ^{157}Gd and ^{155}Gd were analysed assuming s-wave capture and using an average Γ_γ obtained from the Resolved Resonance Region (RRR). From this experiment the values of $\sigma_0^{155} = 62.2 \pm 2.2$ kb and $\sigma_0^{157} = 239.8 \pm 8.4$ kb were extracted for the thermal capture cross section of ^{155}Gd and ^{157}Gd respectively. The resulting Westcott factors were 0.86 ± 4 and 0.89 ± 4 for ^{155}Gd and ^{157}Gd respectively.

2.2 Comparison of data

As shown in the previous section, there are several measurements of the gadolinium thermal cross section. Analysing the results of these measurements we can see how, especially for ^{157}Gd, the data are inconsistent with each other. In Tab.2.10 we can see a comparison of the thermal cross section for both ^{155}Gd and ^{157}Gd from different experiments and libraries. In Fig.2.1 and Fig.2.2 all these cross section data are shown in a timeline.

As we can notice from the previous table there are many inconsistency in the data. For ^{155}Gd the value from Choi differs from the ENDF one more than 7% while for ^{157}Gd Leinweber cross section is 12% smaller than the one in libraries. All these inconsistencies made new measurements of these cross sections necessary. To obtain a precise estimation of ^{155,157}Gd cross sections a transmission measurement using enriched and natural metallic disks was performed at the GELINA facility at the JRC of Geel (Belgium) (see Chapter 3).

Author/Library (year)	^{155}Gd thermal cross section (kb)	Deviation from ENDF	^{157}Gd thermal cross section (kb)	Deviation from ENDF
Möller (1960)	58.9(5)	-3.4%	254(2)	0.3%
Ohno (1968)	61.9(6)	1.6%	248(4)	-2.1%
Leinweber (2006)	60.2	-1.2%	226	-12%
Choi (2014)	56.7(21)	-7.4%	239(6)	-6%
Mughabghab (2009)	60.9(2)	//	254.0(8)	0.3%
JENDL-4.0 (2016)	60.735	-0.5%	253.25	//
JEFF-3.3 (2017)	60.89	//	254.5	0.5%
ENDF/B-VIII (2018)	60.89	//	253.32	//
Mastromarco (2019)	62.2(2.2)	2.1%	239.8(8.4)	-5.6%

Table 2.10: Comparison of thermal cross section of ^{155,157}Gd from different experiments and libraries.

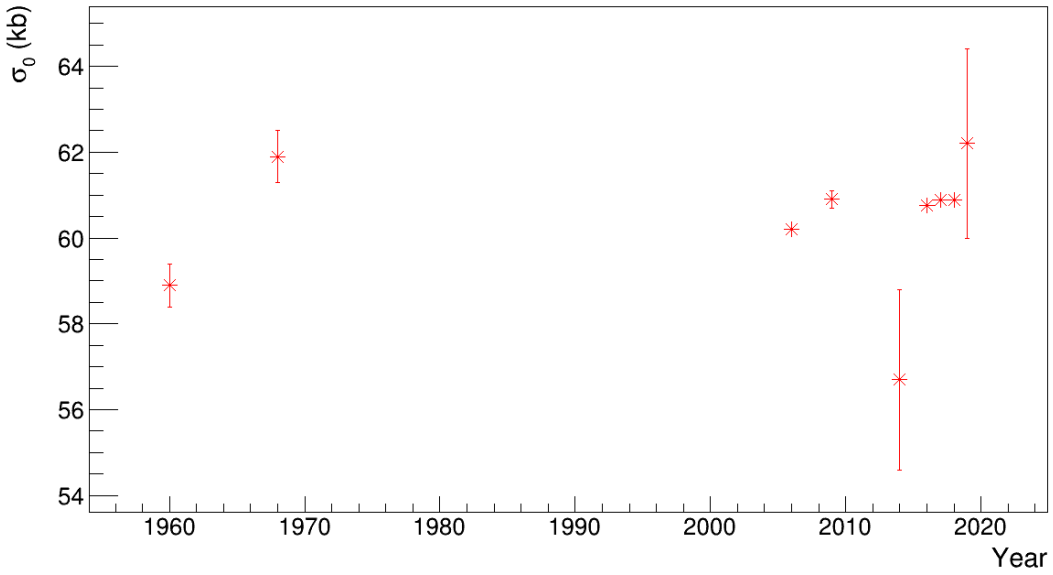

Figure 2.1: Thermal cross section measurements of ^{155}Gd over the years.

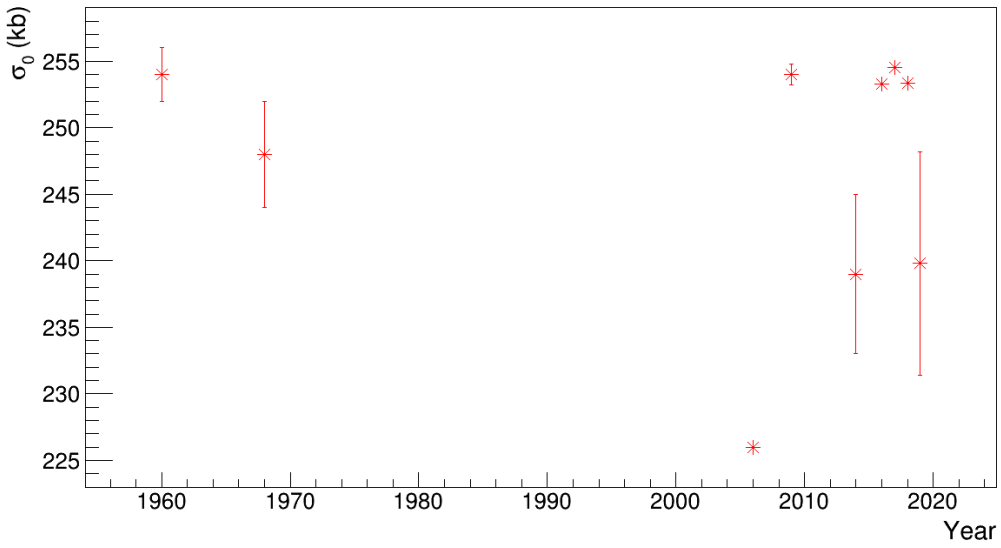

Figure 2.2: Thermal cross section measurements of ^{157}Gd over the years.

The resonance parameters for the lower energy resonances are important as well. In fact, many of the experiments described before obtained also the resonance parameters both in the resolved and the unresolved resonance region. The most important resonance parameters are the energy of the peak and the partial widths (Γ_n and Γ_γ). The widths of resonance are often obtained measuring the kernel of the resonance which is proportional to its area. The kernel is defined as:

$$k = \frac{g\Gamma_n\Gamma_\gamma}{\Gamma_n + \Gamma_\gamma}, \tag{2.6}$$

where g is the statistical spin factor. Therefore the ratio of the kernels from different experiments can help to highlight any systematic inconsistency. The ratio of the kernels of the first resonances of ^{155,157}Gd for some of the experiments described before are shown in Fig.2.3, 2.5 and Fig.2.4, 2.6 as a function of energy and Γ_n respectively. In particular, the resonances below 30 eV and 100 eV were analysed for ^{155}Gd and ^{157}Gd respectively. As we can see from these figures the kernels obtained at RPI are mostly lower than the one measured at n_TOF this year. In Tab.2.11 and Tab.2.12 are listed all the resonance parameters for ^{155}Gd and ^{157}Gd respectively.

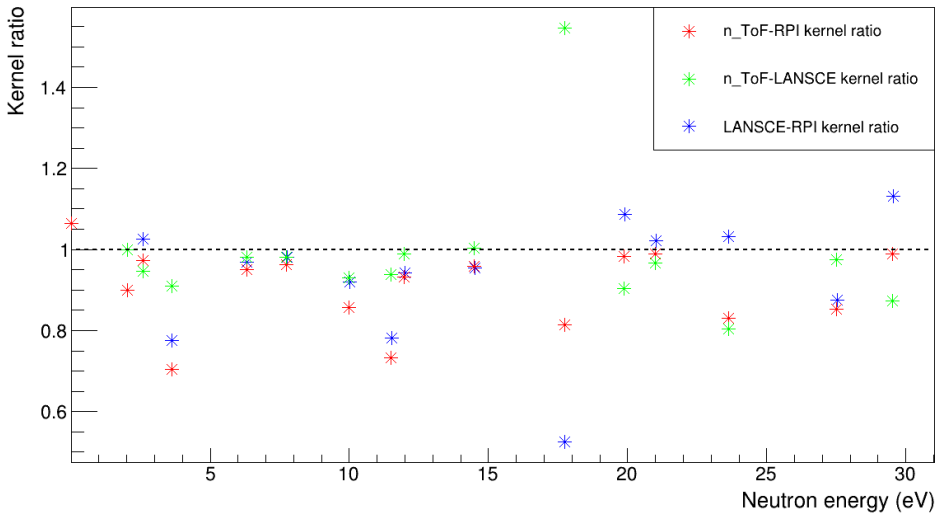

Figure 2.3: Kernel ratio for the ^{155}Gd resonances below 30 eV in function of neutron energy for different facilities. The red stars are the ratio between n_TOF and RPI, the green ones the ratio between n_TOF and LANSCE and the blue ones the ratio between LANSCE and RPI.

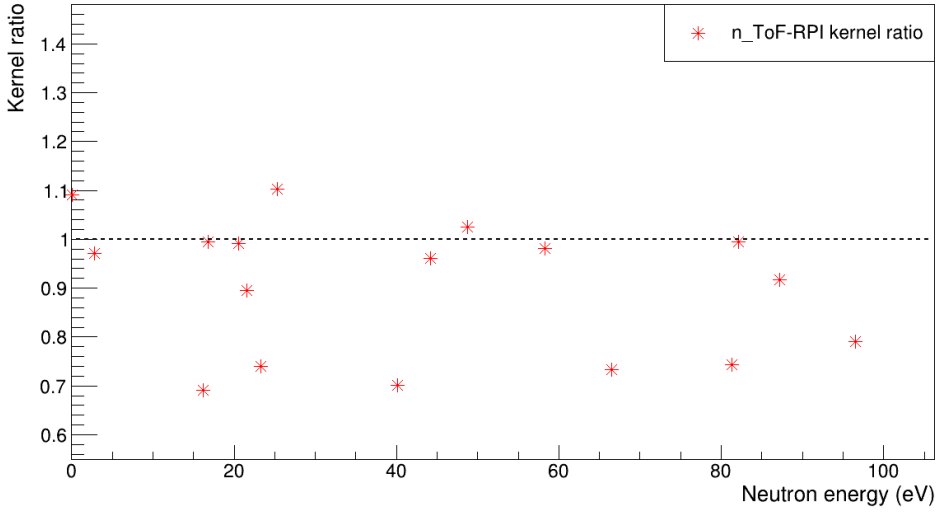

Figure 2.4: Kernel ratio for the ^{157}Gd resonances below 100 eV as a function of neutron energy between n_TOF and RPI.

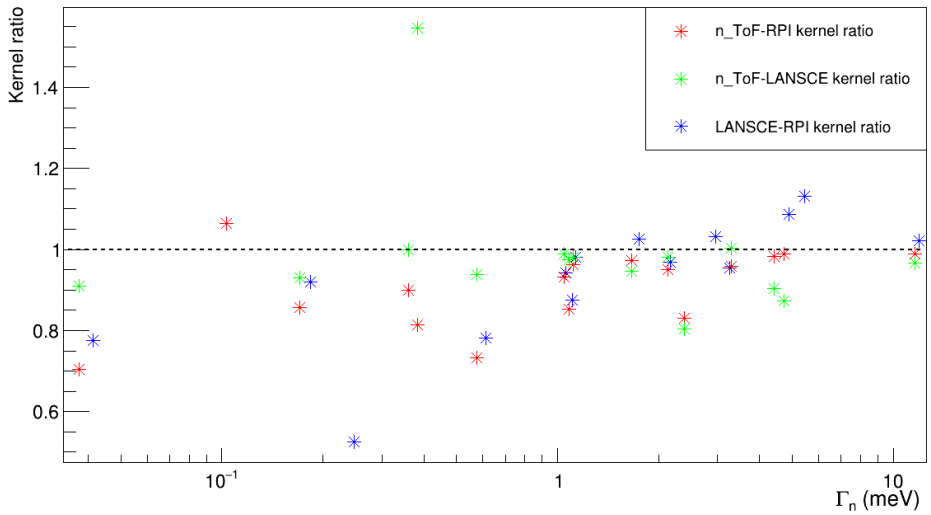

Figure 2.5: Kernel ratio for the ^{155}Gd resonances below 30 eV in function of Γ_n for different facilities. The red stars are the ratio between n_TOF and RPI, the green ones the ratio between n_TOF and LANSCE and the blue ones the ratio between LANSCE and RPI.

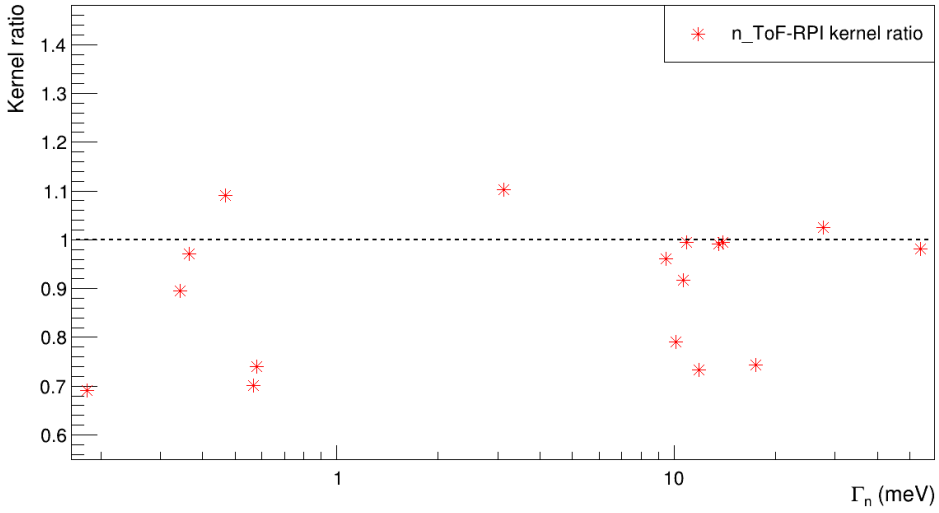

Figure 2.6: Kernel ratio for the ^{157}Gd resonances below 100 eV in function of Γ_n between n_TOF and RPI.

E (eV)				Γ_γ (meV)				$2g\Gamma_n$ (meV)			
ENDF	RPI	LANSCE	n_TOF	ENDF	RPI	LANSCE	n_TOF	ENDF	RPI	LANSCE	n_TOF
0.0268	0.025(3)	n.d	0.0268	108	104(3)	n.d	104.57(8)	0.130	0.121(4)	n.d	0.1288(10)
2.008(10)	2.0120(2)	2.02(1)	2.0128(2)	110(1)	128(1)	112(2)	111.0(6)	0.278(3)	0.30(1)	0.27(1)	0.2700(8)
2.568(13)	2.5729(3)	2.575(10)	2.5730(1)	111(1)	107.1(4)	107(2)	102.8(2)	2.18(2)	2.133(4)	2.19(2)	2.074(2)
3.616(6)	3.616(3)	3.62(3)	3.618(2)	130(17)	130	121(2)	125(7)	0.033(2)	0.04(2)	0.031(2)	0.0282(8)
6.3(2)	6.3057(2)	6.31(1)	6.3062(2)	114(7)	108.8(6)	114(3)	103.6(5)	2.50(15)	2.80(1)	2.71(3)	2.664(6)
7.75(1)	7.7477(4)	7.76(1)	7.7490(4)	124(4)	109(1)	119(4)	102.3(8)	1.40(5)	1.45(1)	1.42(2)	1.396(6)
10.01(1)	9.991(3)	10.02(2)	10.000(2)	115(20)	110(20)	120	102(5)	0.21(2)	0.25(5)	0.23(1)	0.214(4)
11.53(1)	11.508(1)	11.53(3)	11.507(1)	125(23)	120(40)	120	105(4)	0.45(3)	0.59(6)	0.46(1)	0.432(6)
11.99(1)	11.964(8)	11.99(2)	11.9729(7)	112(11)	130(20)	121(5)	107(2)	1.10(5)	1.40(5)	1.32(2)	1.306(8)
14.51(1)	14.476(9)	14.50(2)	14.4851(6)	103(10)	130(10)	126(5)	102(1)	2.4(2)	2.57(7)	2.45(4)	2.476(12)
17.77(2)	17.729(5)	17.73(3)	17.733(2)	120(25)	130(40)	120	97(7)	0.31(2)	0.59(5)	0.31(2)	0.48(1)
nd	nd	17.81(3)	nd	nd	nd	120	nd	nd	nd	0.23(2)	nd
19.92(2)	19.86(1)	19.91(3)	19.8790(6)	104(16)	118(6)	120	107(1)	5.7(4)	5.6(1)	6.1(10)	5.52(2)
21.03(4)	20.97(2)	21.01(2)	20.9902(4)	98(6)	140(20)	130(4)	121(1)	19.5(9)	14.5(6)	14.93(3)	14.5(4)
nd	22.32(1)	22.45(2)	nd	nd	127	126(4)	nd	nd	0.41(3)	0.28(5)	nd
23.67(4)	23.592(3)	23.62(3)	23.626(1)	120(15)	120	120	94(6)	3.9(1)	3.58(8)	3.7(6)	2.98(4)
27.57(5)	27.482(7)	27.55(5)	27.519(3)	125(20)	125	120	101(8)	0.84(2)	0.95(5)	0.83(2)	0.81(18)
29.58(5)	29.519(3)	29.54(6)	29.528(1)	108(22)	108	120	112(3)	5.4(4)	6.0(1)	6.8(3)	5.92(6)

Table 2.11: ^{155}Gd resonance parameters for E_n <30 eV from four different database

E (eV)			Γ_γ (meV)			$2g\Gamma_n$ (meV)		
ENDF	RPI	n_TOF	ENDF	RPI	n_TOF	ENDF	RPI	n_TOF
0.0314	0.032(3)	0.0314	106	107(3)	111.80(2)	0.58	0.535(5)	0.5842(2)
2.825	2.8287(4)	2.8290(1)	97	109.7(9)	105.9(3)	0.431	0.471(5)	0.4572(8)
16.24	16.201(5)	16.219(2)	91	130(30)	117(8)	0.3	0.33(3)	0.228(6)
16.77	16.78(1)	16.7946(2)	81	112(7)	102.8(5)	16.0	17.38(6)	17.46(6)
20.56	20.51(2)	20.5262(3)	114	114	98.8(6)	14.3	16.8(5)	16.94(4)
21.65	21.60(1)	21.601(2)	121	121	88(6)	0.5	0.48(3)	0.430(8)
23.33	23.27(1)	23.290(2)	121	121	94(5)	0.6	0.59(3)	0.436(6)
25.4	25.349(3)	25.3653(8)	85	85	99(2)	2.30	2.138(5)	2.352(14)
40.17	40.11(1)	40.091(3)	110	110	84(7)	1.0	1.01(5)	0.708(12)
44.22	44.104(2)	44.1374(8)	96	96	101(2)	11.20	12.4(3)	11.8(6)
48.8	48.685(2)	48.7076(6)	90	108(5)	99(1)	30	32.8(9)	34.6(2)
58.38	58.252(2)	58.2927(1)	101	117(12)	104(2)	35	39.1(3.9)	40.2(2)
66.65	66.479(4)	66.536(1)	67	95(5)	100(3)	11.00	12.8(3)	8.90(3)
81.48	81.240(4)	81.312(2)	108	108	121(5)	15	19(2)	13.08(10)
82.3	82.04(1)	82.103(3)	85	85	91(7)	7.7	8.3(9)	8.18(10)
87.46	87.099(4)	87.175(2)	128	128	78(4)	12.8	13.9(1.4)	13.32(12)
96.6	96.488(5)	96.572(2)	110	110	78(4)	25.4	15.8(1.6)	12.66(14)

Table 2.12: ^{157}Gd resonance parameters for E_n <100 eV from three different database

Chapter 3

Experimental details

In this chapter, I explain all the experimental details of the transmission measurements performed at GELINA on gadolinium samples. After the description of all the samples used in the measurements, I outline the TOF technique used at GELINA for the measurement of neutron energy. Moreover, the technical characteristics of the transmission experiment and of the facility, as the neutron production mechanism and the detection stations, are presented.

3.1 Gadolinium samples

Nine samples were used in this measurement campaign. Four were metallic disks, enriched in ^{155}Gd and ^{157}Gd of two different thicknesses. These samples will be called in the following ^{155,157}Gd thin and thick. The enriched samples were produced by the Oak Ridge National Laboratory (USA) and were used in the capture measurement performed at n_TOF last year [1]. These samples are highly enriched in the required isotope and they have very small contamination of other isotopes. All these samples are 30 mm disks and all of them have a mylar substrate of known thickness. A sample enriched in ^{154}Gd was also used in this experiment. Like the samples enriched in ^{155,157}Gd, this sample was produced by the Oak Ridge National Laboratory in the shape of a metallic disk of 30 mm of diameter. In Tab.3.1 is shown the isotopic composition of these enriched

samples. The isotopic composition is the same for both thin and thick samples. The uncertainty on the isotopic abundances is below 0.2%, according to the provider. The other characteristics of the samples like mass and areal density are shown in Tab.3.2.

Sample	^{152}Gd	^{154}Gd	^{155}Gd	^{156}Gd	^{157}Gd	^{158}Gd	^{160}Gd
^{nat}Gd	0.20	2.18	14.80	20.47	15.65	24.84	21.86
^{154}Gd	$< 0.05\%$	66.78%	17.52%	7.23%	3.16%	3.44%	1.87%
^{155}Gd	0.03%	0.63%	91.74%	5.12%	1.14%	0.94%	0.4%
^{157}Gd	$< 0.01\%$	0.04%	0.29%	1.68%	88.32%	9.10%	0.57%

Table 3.1: Isotopic composition of ^{155,157}Gd enriched thin and thick samples, ^{154}Gd enriched sample and natural gadolinium.

Sample	Mass (mg)	Areal density (atoms/b)
^{154}Gd	263.5 (1)	1.452 (5) $\times 10^{-4}$
^{155}Gd Thin	10.0 (1)	1.236 (12) $\times 10^{-5}$
^{155}Gd Thick	100.6 (1)	1.2440 (40) $\times 10^{-4}$
^{157}Gd Thin	4.7 (1)	5.74 (12) $\times 10^{-6}$
^{157}Gd Thick	191.6 (1)	2.3390 (60) $\times 10^{-4}$
MgGd 0.8mm	2560	1.3695 $\times 10^{-6}$
MgGd 1.5mm	4888	2.6158 $\times 10^{-6}$
MgGd 2mm	6153	3.2889 $\times 10^{-6}$
MgGd 3mm	9473	5.0657 $\times 10^{-6}$

Table 3.2: Mass and areal density of the measured samples.

Together with the enriched samples, a set of four natural gadolinium disks were used. These disks were magnesium alloys with a 0.25% wt of natural gadolinium. The samples used in this experiment had the same concentration of gadolinium but different thicknesses. In the following the different samples will be then distinguished by their thickness (0.8 mm, 1.5 mm, 2 mm, and 3 mm). These samples were specially produced

for this experiment by the University of Leoben (Austria). The characteristics of these samples are listed in Tab. 3.2. All these values were measured at the JRC of Geel. The area was determined by an optical surface inspection with a microscope system from Mitutoyo [28].

3.2 Time-of-flight technique

To measure neutrons' kinetic energy at GELINA the time-of-flight (TOF) technique is used. To perform TOF measurements the neutron beam must be pulsed. The measured time-of-flight is defined as the difference between the time of detection in the transmission detector t_d and the start time t_0 given by the passage of charged particles in one of the last coils of the accelerator. The measured time-of-flight is then defined as:

$$t_m = t_s - t_0. \tag{3.1}$$

In time-of-flight facilities, the neutron beam is usually produced by the collision of an electron- or proton-beam with a thick neutron-producing target (e.g. U, W or Pb). Together with neutrons, many γ-rays are produced in the collisions. These γ-rays travel inside the beam pipe at the speed of light and reach the detector, causing a detected signal that often saturates the detection system. This signal is called gamma-flash. The gamma-flash is used to measure the time offset in the measured time t_m:

$$t = t_m - (t_\gamma - L/c), \tag{3.2}$$

where t_γ is the time difference between the gamma-flash and t_0, L is the flight-path length and c is the speed of light.

The kinetic energy of neutrons can be expressed relativistically as:

$$E_n = E_{tot} - mc^2 = \sqrt{(c^2p^2 + m^2c^4)} - mc^2 = mc^2(\gamma - 1), \tag{3.3}$$

where $\gamma = (1 - v^2/c^2)^{-1/2}$ is the Lorentz factor. The first term of the series expansion gives us the classical expression for kinetic energy:

$$E_n \approx \frac{1}{2}mv^2 = \left(\alpha\frac{L}{t}\right)^2. \tag{3.4}$$

Using $c = 2.99792458 \times 10^8 m/s$ and $m = 939.6 MeV/c^2$ we obtain $\alpha \approx 72.298$ when L is expressed in meters, t in microseconds and E_n in eV. From the relativistic expression of kinetic energy we obtain that the energy resolution is given by:

$$\frac{\Delta E}{E} = (1+\gamma)\gamma\frac{\Delta v}{v} = (1+\gamma)\gamma\sqrt{\left(\frac{\Delta t}{t}\right)^2 + \left(\frac{\Delta L}{L}\right)^2}, \tag{3.5}$$

which, at non-relativistic energies, can be expressed as:

$$\frac{\Delta E}{E} \approx 2\frac{\Delta v}{v} = 2\sqrt{\left(\frac{\Delta t}{t}\right)^2 + \left(\frac{\Delta L}{L}\right)^2}. \tag{3.6}$$

Usually, Δt is the quadratic sum of the initial burst width uncertainty and electronic time resolution. At GELINA the initial burst has a FWHM of 1 ns. ΔL is a sum of the flight path uncertainty and an additional term given by the moderator effect. In fact, the neutrons do not escape instantaneously form the moderator and the moderation time is not constant. Studying with Monte Carlo codes the probability distribution of the time spent inside the moderator we can see that it is easier to perform a transformation of variables from a time (t_t) to an equivalent distance (L_t):

$$L_t = vt_t \tag{3.7}$$

where v is the escaping velocity of the neutron. From previous simulation we can see that the equivalent distance distribution is almost constant for different neutron energies. At GELINA, the FWHM of the equivalent distance distribution is 2 cm, about half of the moderator thickness. The flight path uncertainty is $\approx$ 1 mm. Using these values is possible to estimate the energy resolution at the 10.86 m flight path with respect to neutron energy. The calculated resolution is shown in Fig.3.1.

3.3 Transmission principle

Transmission is the simplest and more accurate type of cross section measurements. The transmission factor T is defined as the percentage of neutrons that traverses the sample without interacting with it. It is related to the total cross section by:

$$T = e^{-n\sigma_{tot}} \tag{3.8}$$

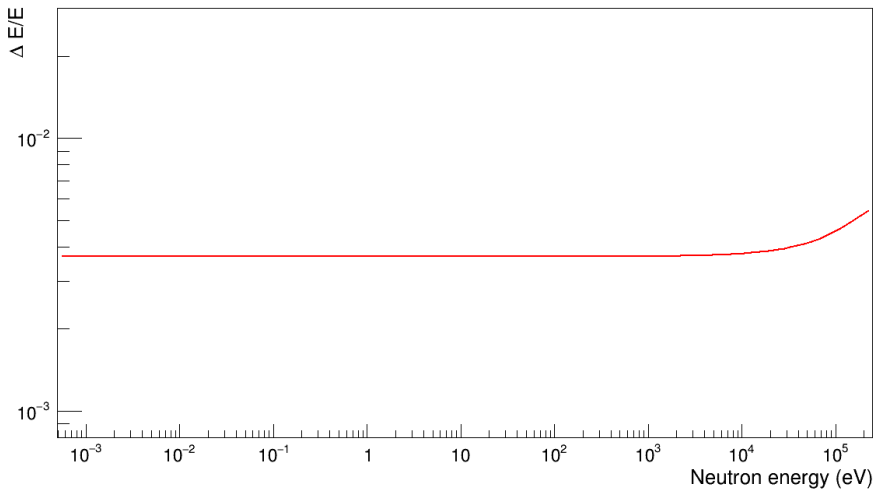

Figure 3.1: Energy resolution of GELINA at the 10.86 m flight path

where n is the areal density of the sample expressed in atoms/barn. Experimentally, transmission is obtained as a ratio of sample-in and sample-out counts both corrected for their respective background

$$T_{exp} = \frac{C_{in} - B_{in}}{C_{out} - B_{out}}. \tag{3.9}$$

The experimental transmission T_{exp} can be related to the total cross section only if:

1. the target is perpendicular to the neutron beam
2. all the detected neutrons have crossed the target
3. scattered neutrons are not detected

To fulfill these condition good collimation in a small solid angle of the neutron beam is necessary near the sample. Moreover, a homogeneous target is fundamental to correctly relate T_{exp} to the total cross section.

Thanks to the definition of T_{exp} in Eq.3.9, the neutron fluence together with detector efficiency cancels out in the measurement. In addition, corrections for multiple scattering are not necessary. The main difficulties in transmission experiments are related to the

background estimation. In fact, the background has to be measured using black resonance filters [27] that covers the entire energy range of interest. For energies below 1 eV, the background level can only be extrapolated from the observed background at higher energies. Moreover, the background level at the detection position is affected not only by the sample but also by the filters. Therefore a separate measurement of sample-in and sample-out background is necessary.

3.4 GELINA facility

The Geel Electron Linear Accelerator (GELINA) is a neutron time-of-flight facility located in the Joint Research Center (JRC) of Geel (Belgium) [29]. This facility was built in 1965 and upgraded many times during the years. GELINA was designed for high-resolution cross section measurement in a wide energy range, between 10 meV and 20 MeV. It is a multi-user facility capable of serving up to 10 different experiments at once. Fig.3.2 shows an aerial picture of the facility.

3.4.1 Neutron production

The production of the neutron beam starts with the acceleration of the electrons inside the LINAC. The electrons are generated in an injector with a triode gun in 10 ns pulses. The accelerator consists of three sections operating at 2999 MHz. The maximum repetition rate of the accelerator is 800 Hz and the energy of the electron pulse leaving the accelerator varies linearly from 140 MeV at the start of the pulse to 70 MeV at the end of the pulse. Before colliding with the neutron production target, the electrons make a 'looping' in a compression magnet. The magnet consists of five magnetic sectors and it is designed to accept the 50% electron energy spread in the beam. The more energetic electrons will have a higher bending radius and therefore they will be delayed with respect to the less energetic electrons. Using this principle is possible to compress a 10 ns electron pulse to a 1 ns time bin.

After the compression magnet, the electron pulse collides with a rotating neutron-

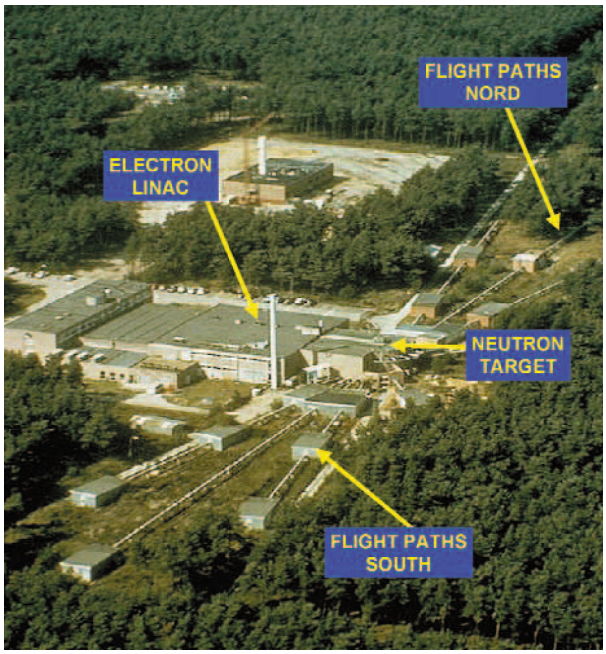

Figure 3.2: Aerial picture of GELINA. All the vacuum tubes of the different flight-path are visible.

producing target. The target consists of a U-Mo alloy with 10%wt of molybdenum cooled with liquid mercury and sealed in stainless steel. Inside the target, the electrons are decelerated and produce high-energy Bremsstrahlung photons. These photons will then interact with the target nuclei and produce neutron via photo-reaction (γ,n) or, to a lesser extent, photo-fission (γ,f). From a thick uranium target, roughly 6 neutrons are emitted per 100 electrons of 100 MeV. The power density deposited in the target by the electron beam can reach 10 kW/cm^3. To avoid localized heating in the target it is mounted over a rotating mechanism. The mercury coolant was chosen to avoid neutron moderation. Fig.3.3 shows a scheme of the neutron-producing target.

The target produces on average 3.4 $\times 10^{13}$ neutron/s. To increase the neutron flux in the energy range below 100 keV two water-filled moderators are placed above and below the target. The partially moderated neutrons have an approximate 1/E energy dependence and a Maxwellian peak at thermal energy. Two flux configuration are possible: one optimised for energy below 500 keV with neutron coming from the moderator and

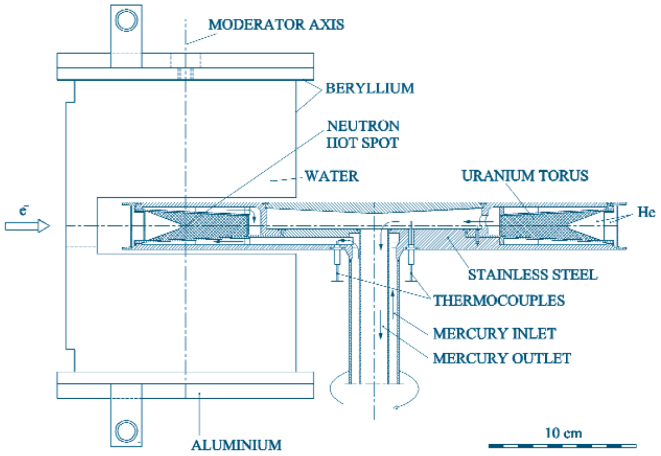

Figure 3.3: GELINA's rotating neutron-producing target scheme.

one with fast neutrons ($\approx$ MeV) using the non moderated beam. To shield the unwanted neutrons in a particular flight path, shadow bars are properly placed between the source and the flight path. Further tailoring of the spectral shape is done with movable filters. The produced neutron beam is continuously monitored using BF_3 proportional counters mounted on the ceiling of the target hall. These detectors are also used to normalize the measured neutron spectra to the same neutron intensity. [29]

3.4.2 Experimental areas

The neutron beam, direct or moderated, is isotropically emitted and enter the 12 different flight paths. The flight tubes are under vacuum, they have a diameter of 50 cm and their lengths range up to 400 m. There are several measurement stations at different distances from the target (nominal distances are 10, 30, 50, 60, 100, 200, 300 and 400 m). Depending on the distance from the target we have a different neutron flux due to its $1/L^2$ dependency. Fig.3.4 shows a scheme of the flight path and experimental areas of GELINA.

Transmission experiments can be performed at different flight paths using Li-glass [30] or plastic scintillators [31]. To study the Doppler broadening one of the measurement

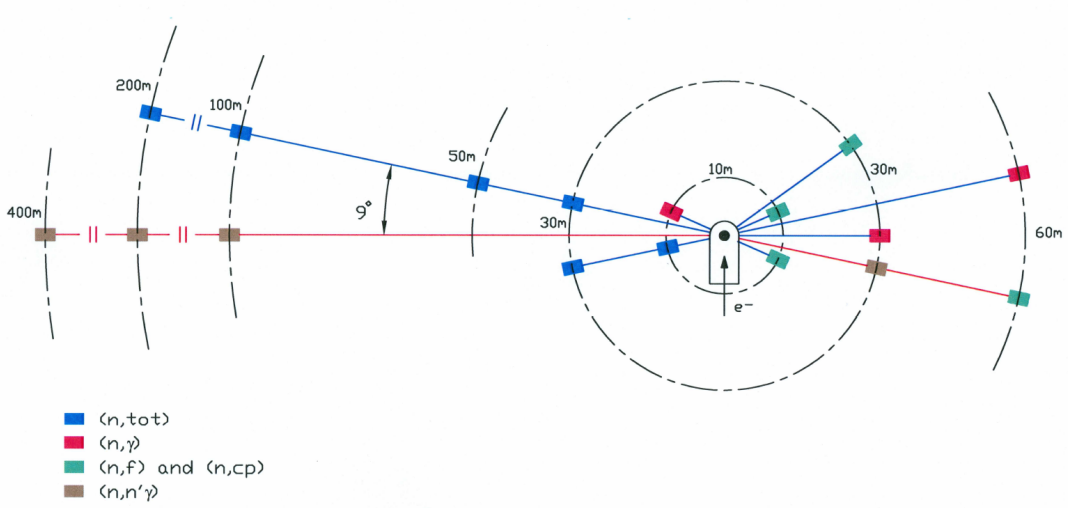

Figure 3.4: Flight path and experimental areas of GELINA. In blue we have the transmission stations, in red radiative capture, in green fission, and in brown inelastic scattering.

stations is equipped with a cryostat that can cool down the sample to 10 K [32]. For radiative capture measurements, C_6D_6 scintillators are used. They are calibrated using standard γ-ray emitters and the calibration is monitored using a Th sample once a week. Fission cross section measurements are performed using Frisch gridded ionization chambers [33]. These stations are also used to study neutron-induced charged particle reactions [34]. Reactions like (n,xnγ) are studied using HPGe detectors [35].

3.5 Experimental conditions

All the measurements described in this work were carried out at the GELINA facility between May 2018 and June 2019 with a flight path length of 10.860 m (Flight Path 13). The flight path forms an angle of 18° with the direction normal to the moderator. The transmission was measured using ^{6}Li glass scintillators produced by Scionix [36]. The moderated neutron spectrum was used. A set of Pb, Ni and Cu annular collimators was used to reduce the neuron beam to a diameter of 10 mm at the sample position. The

Sample	Frequency
^{155,157}Gd Thin	50 Hz
^{155,157}Gd Thick	400 Hz
^{154}Gd	400 Hz
MgGd alloys	50 Hz

Table 3.3: Accelerator frequencies used for different samples

samples and detectors were placed in an acclimatized room to keep the temperature constant at 20°C thus avoiding electronic drifts. Sample-in and sample-out measurements were performed using a sample changer that allows switching between the two configurations remotely. The measurements were divided into many short duration cycles ($\approx$ 600 s) alternating different configurations of samples and filters. For all the enriched samples the sample-out measured was performed using a mylar target of the same thickness and characteristics of the sample's substrate to subtract its effect in transmission. The same procedure was used for 1.5 mm, 2.0 mm and 3.0 mm MgGd alloys using a pure magnesium sample of the same thickness as the alloys. For 0.8 mm MgGd alloy the sample-out was measured without any sample in the beam.

Permanent Na and Co black resonance filters are placed in the beam to monitor the background level at 2850 eV and 132 eV. Additional W, Ag and Rh filters were used in some cycles to measure the background level at lower energies. Only cycles for which the neutron monitor counts deviated by less than 1% with respect to the average of the previous and the subsequent cycle were selected.

Accelerator frequencies ranging between 400 Hz and 50 Hz were used. For measurement at 400 Hz a B overlap filter was used to absorb slow neutrons from a previous burst. In Tab.3.3 the frequencies used for each sample are shown.

Chapter 4

Analysis

In this chapter, I present the acquisition system and the data reduction and analysis procedure performed on the measured sets of data. The data reduction was carried out using the AGS (Analysis Geel Spectra), developed at JRC-Geel to transform the count rate spectra of time-of-flight measurements into experimental observables (e.g. transmission). The data analysis was performed using the R-Matrix fitting program REFIT.

4.1 Detection system

At GELINA the transmission measurements are performed using Li-glass scintillators. Lithium is used to detect slow neutrons by using the reaction:

$$^{6}Li + n \rightarrow \alpha(2.73MeV) +^{3} H(2.05MeV), \tag{4.1}$$

which has a total cross section of 941 b at thermal energy and a nearly featureless $1/v$ behaviour for energies up to hundreds of keV. The detector used at the 10 m flight-path (FP-13) is a rectangular shaped scintillator produced by Scionix [36]. This scintillator is enriched to 95% in ^{6}Li to increase the detection efficiency. It is enclosed in aluminium canning surrounded by a solid $\mu-$metal shield and the built-in voltage divider presents one anode and one dynode outputs. In the acquisition system, both the anode and

dynode signal are used. The anode signal is very fast hence it is used to determine the TOF while the dynode signal (9^{th} dynode on 14 stages PMT) is proportional to the light produced by the scintillator and can be used to obtain the amplitude spectrum.

The anode signal is directly transmitted to a constant fraction discriminator (CFD) which produces a logic signal when the pulse reaches a given fraction of the total pulse. This logic signal (STOP) is then sent to the TDC to determine the time-of-flight with respect to the t_0 produced by the coils of the LINAC (START) (see section 3.2). The dynode signal is first shaped by a pre-amplifier (PA) and subsequently amplified by a spectroscopic amplifier (SA) to produce the final amplitude signal. Before the digitalization, this signal passes through a linear gate that transmits the signal only if a valid time-of-flight output was produced. After the gate, the signal is digitized by an ADC. These signal are then sent to the DAQ system, a Labview based application which stores all the produced time-of-flight and amplitude signals in list files [37].

The energy calibration of this scintillator was performed using ^{137}Cs and ^{207}Bi sources. Measuring the response of the scintillator and knowing the position of the Compton edge for these sources, it was possible to calibrate the detector in the energy range between 500 keV and 1800 keV. The time resolution of the scintillator was directly measured using a ^{60}Co source, which emits two γ-rays in coincidence. Using two scintillators it was possible to obtain a FWHM of 4.21 ns. In Fig.4.1 is shown a picture of the detector.

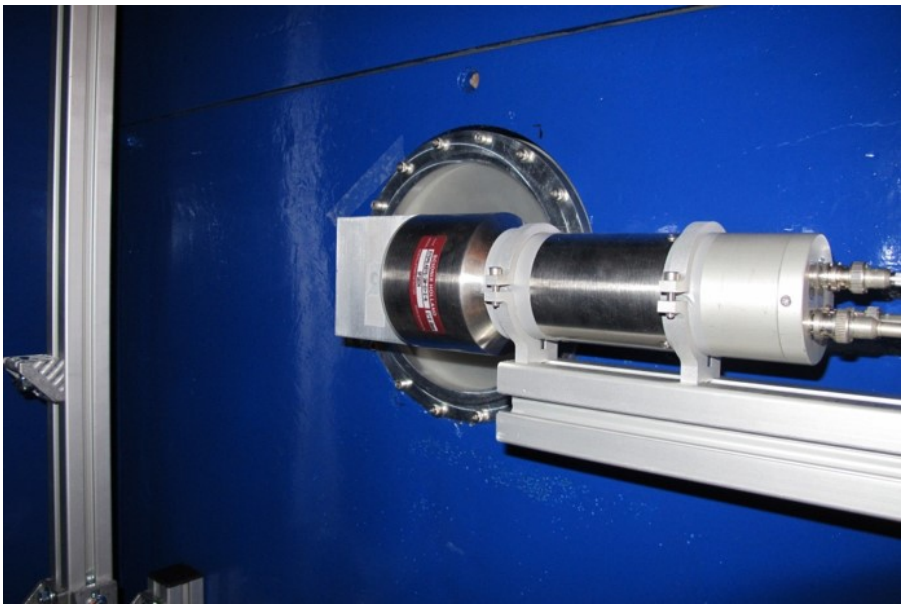

Figure 4.1: Picture of the Li-glass scintillator used at FP-13 for transmission measurements.

4.2 ADC gain shift

During the first part of the data analysis, a deviation was observed in the gain factor of the ADC connected to the lithium scintillator. This shift was observed in about 1/3 of the cycles of ^{155}Gd-thin sample measurement at 50 Hz and, to a far less extent, in ^{157}Gd-thin sample measurement at 50 Hz. This effect disappeared after these measurements. To avoid a potential mismatch between the data with different gain, only the non-shifted ones were selected. In this way, although we lost some statistics, it was possible to obtain a consistent dataset. In Fig.4.2 and 4.3, the amplitude spectra before and after the event selection are shown. The black line represents the complete set of recorded data while the red one is the spectrum of the selected events. As we can see from these figures, the shifted cycles in ^{157}Gd measurement was a little percentage ($\approx 15\%$) while the effect was bigger for ^{155}Gd ($\approx 35\%$).

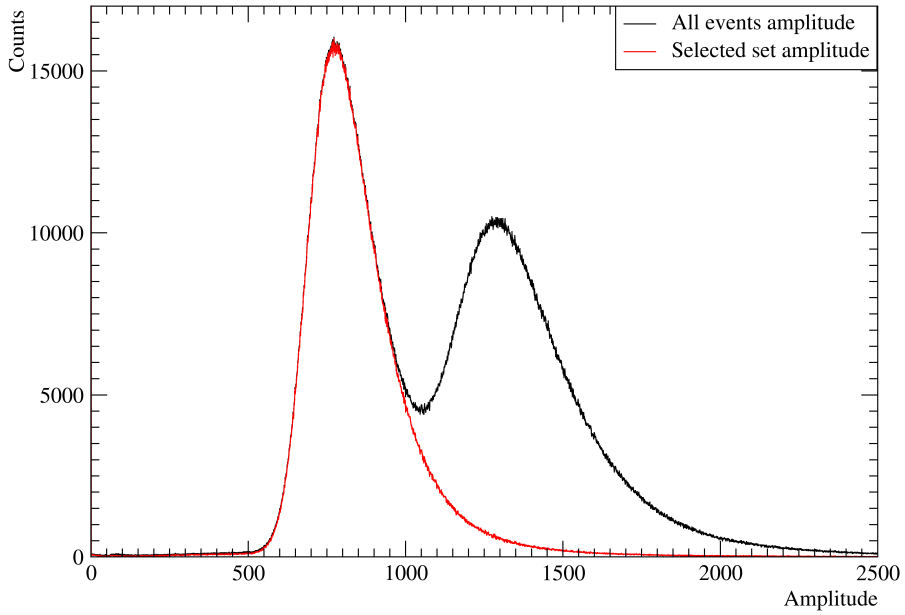

Figure 4.2: Signal amplitude of ^{155}Gd-thin sample before (black) and after (red) event selection

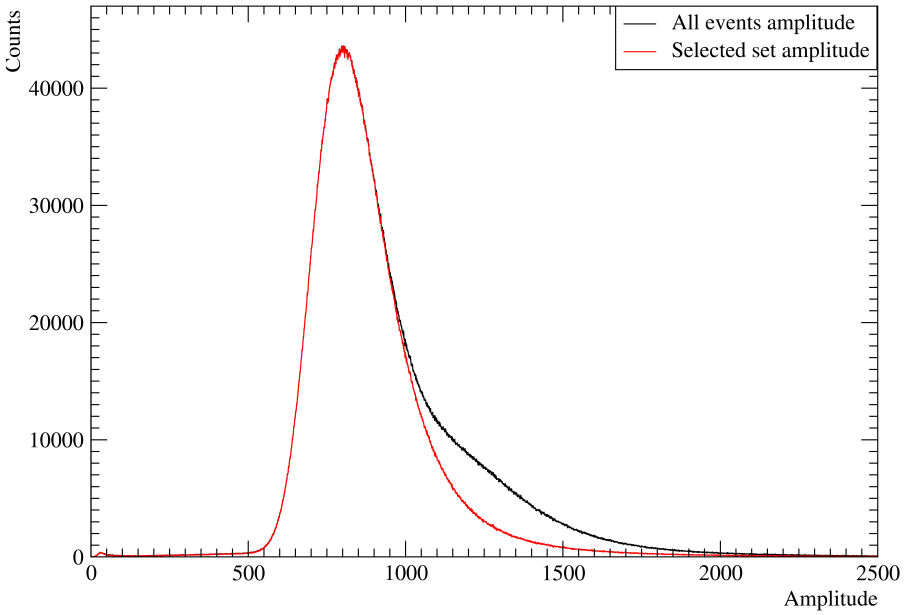

Figure 4.3: Signal amplitude of ^{157}Gd-thin sample before (black) and after (red) event selection

4.3 Data reduction

The data reduction procedure was performed using the AGS (Analysis Geel Spectra) code. This code was developed at IRMM to transform amplitude or TOF spectra into observables like the transmission. The code is based on a compact formalism to propagate all uncertainties, starting from uncorrelated ones due to counting statistics.

4.3.1 Transmission

The experimental transmission T_{exp} is obtained from the ratio of a sample-in measurement C_{in} and a sample-out measurement C_{out}, corrected for their background B_{in} and B_{out} respectively:

$$T_{exp} = N\frac{C_{in} - KBin}{C_{out} - KB_{out}} \tag{4.2}$$

The TOF spectra were corrected for dead time losses in the detector and electronics chain. The dead time is a small correction in the region of interest of this work (below 100 eV). More details on this correction are given in Section 4.3.3. All the spectra were normalized to the same bin-width and neutron intensity. The latter was derived using the information of the BF_3 beam monitor. To avoid systematic effects due to slow variation of the beam both sample-in and sample-out measurements were divided into many cycles of about 600 seconds each. Such procedure reduces the uncertainty on the normalization to less than 0.25%, as shown in previous measurements performed at GELINA [38]. The latter was derived from the ratio of the counts in the Li detector and the flux monitors. The normalization factor $N = 1.0000(25)$ was then introduced in Eq.4.2 to account for this uncertainty. The background was determined by an analytical expression using the black resonance filters technique. To account for correlated uncertainties due to the background estimation, the factor $K = 1.00(3)$ was introduced in Eq.4.2. Its uncertainty was derived from a statistical analysis of the difference between the observed black resonance dips and the estimated background, as discussed in Section 4.3.4.

4.3.2 Time-offset and flight-path length

As discussed above, the time-of-flight of a neutron creating a signal in the detector was determined as the difference between the start T_0 and stop T_s signal:

$$t = (T_s - T_0) - t_0 \tag{4.3}$$

where t_0 is a time-offset introduced by the electronics chain. This offset was measured using the signal coming from the γ flash. The time difference between the observed γ flash and the expected one, obtained as the ratio between the nominal flight-path length and the speed of light, was used as t_0. This procedure was used for all the measurements except for the ^{154}Gd one. In fact, the time shifts observed for two sequential runs were not compatible with the measured one.The time difference among these runs estimated using the γ flash was about 50 ns. As we can see from Fig.4.4 the measured time difference is much higher, at least 150 ns. This inconsistency was caused by the non-linearity of the TDC with very short time measurements.

To obtain the real-time shift between these experiments the 5.91 keV resonance of aluminium was used. Aluminium is present in the vacuum tubes and therefore its effect is visible for every configuration in the TOF spectrum. In particular, to avoid effects related to the samples, we used the "open beam" configuration, which is the configuration with no samples in the beam. Fitting the position of this narrow resonance using a Gaussian curve it was possible to estimate the centre of the resonance with good precision. The time shift was then obtained as the difference of the measured time-flight and the expected one, calculated using the nominal energy (5.906 keV) and flight-path length (10.860 m). The time difference obtained using this technique was 165 ns, perfectly compatible with the observed value. The good agreement of this result with the experimental data is shown in Fig.4.5. This method was also used with ^{155}Gd-thin samples to check its accuracy. The resulting time offset was 45 ns, the same obtained with the γ flash.

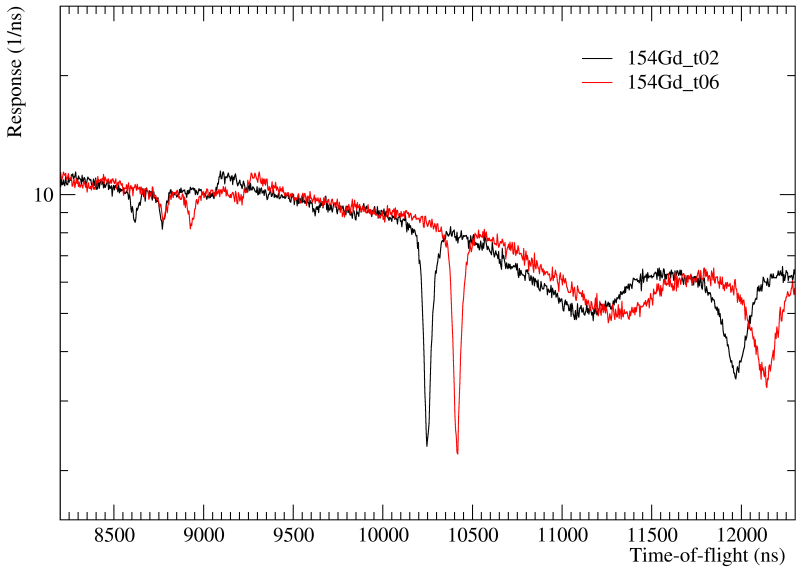

Figure 4.4: 5.9keV Al resonance observed in open beam configuration in two subsequential measurement with ^{154}Gd sample without a time offset correction.

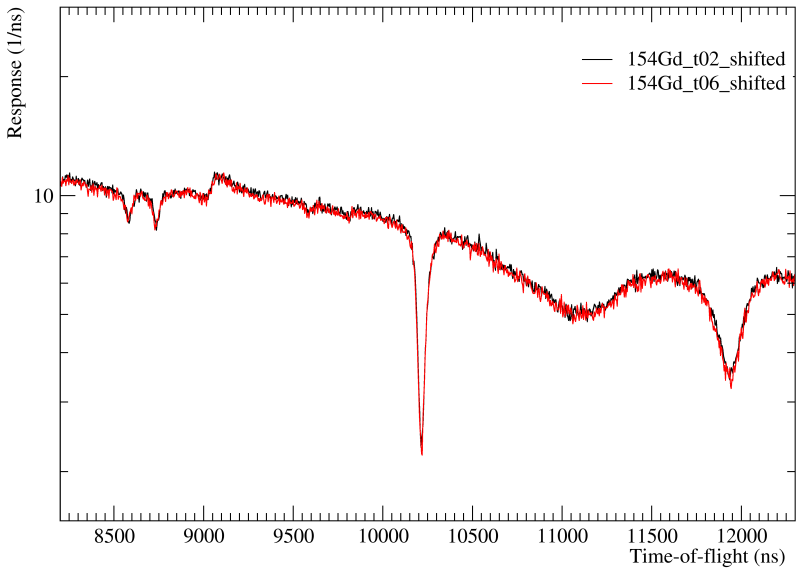

Figure 4.5: 5.9keV Al resonance observed in open beam configuration in two subsequential measurement with ^{154}Gd sample with the time offset correction.

The flight path distance $L = 10.860(1)$ m, i.e. the distance between the centre of the moderator viewing the flight path and the front face of the detector was derived previously from an analysis of transmission data for ^{238}U using the 6.673(1) eV resonance [39].

4.3.3 Dead time correction

The dead time correction is based on the formula of Moore [40], which account for possible variations of neutron beam intensity. As we can see from Fig.4.6 the maximum dead time correction was less than 20%. For neutron energies below 130 keV, which is the region of interest for this work, the correction factor is less than 1.10. It has been demonstrated that the bias effect resulting from such corrections are negligible [27]. The dead time used for all the measurements was $t_d = 3510 \pm 10$ ns.

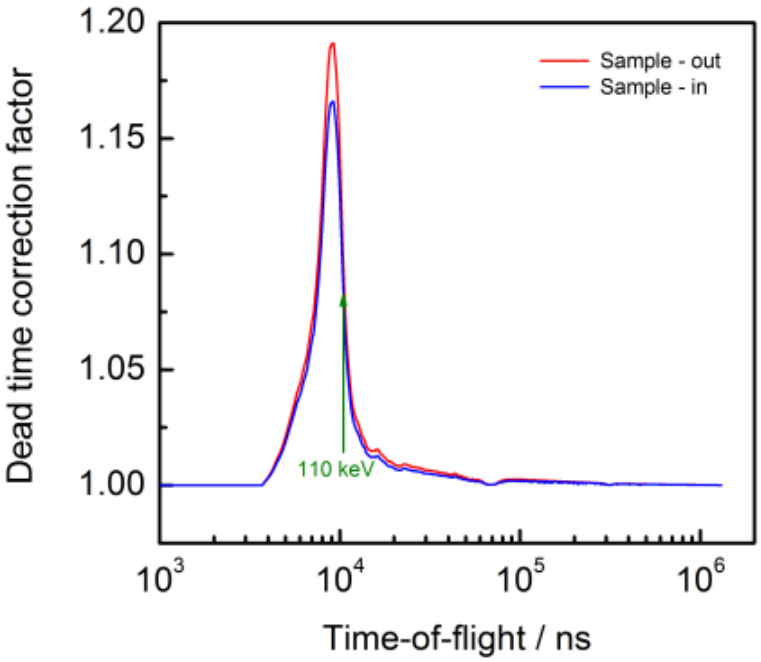

Figure 4.6: Dead time correction factor as a function of time-of-flight for both the sample-in and sample-out measurements.

4.3.4 Background correction

The background as a function of the time-of-flight was parametrized analytically using the following expression:

$$B(t) = b_0 + b_1 e^{-\lambda_1 t} + b_2 e^{-\lambda_2 t} + b_3 e^{-\lambda_3 (t+\tau_0)} \tag{4.4}$$

The parameter b_0 is the time-independent contribution. The first exponential is due to the detection of 2.2 MeV γ-rays resulting from neutron capture in the hydrogen of the moderator. The time dependence of this component was verified by Monte Carlo simulation and confirmed by measurement with polyethylene filters. The second exponential is caused by neutrons scattered inside the detection station. The last time-dependent component accounts for the contribution due to slow neutrons from the previous accelerator cycle. It was approximated by an exponential with τ_0 being the inverse of the accelerator operating frequency (e.g. $\tau_0 = 1.25$ ms at 800 Hz). b_3 and λ_3 were estimated by an extrapolation of the TOF-spectrum at the end of the cycle fitting the least energetic part of the spectrum with a single exponential. An example of these fits is shown if Fig.4.7.

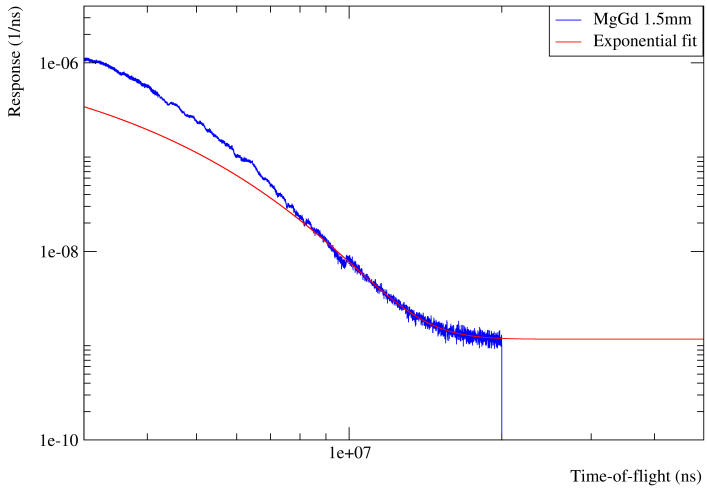

Figure 4.7: Tail of the time-of-flight spectrum of the 1.5 mm MgGd sample at the higher time (blue) and exponential fit (red) used to obtain b_0, b_3 and λ_3 background parameters.

The time dependence of the background was derived from dedicated measurements with Na, Co, W, Ag, and Rh fixed black resonance filters. During the regular sample-in and sample-out runs only Na and Co filters were placed in the beam to continuously monitor the background at 2.85 keV and 132 eV. The dead-time corrected sample-in TOF spectra together with all the background components are shown in Fig.4.8 and Fig.4.9 for all filters (Na, Co, W, Ag, and Rh) and Na, Co filters configuration respectively. In Tab.4.1 are listed all the background parameters used for the different measurements.

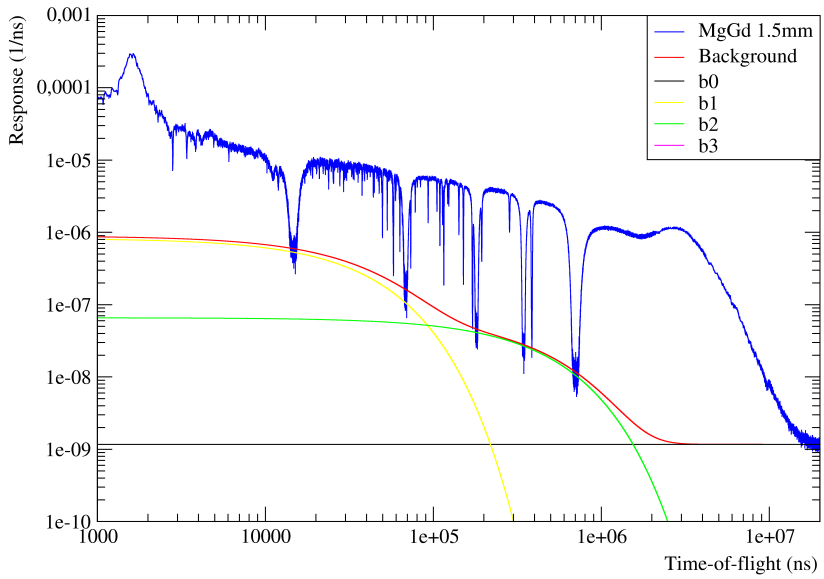

Figure 4.8: Time-of-flight spectrum with the 1.5mm MgGd alloy in the beam with Na, Co, W, Ag, and Rh filters (blue) together with the total background (red). The different contributions to the background are also given.

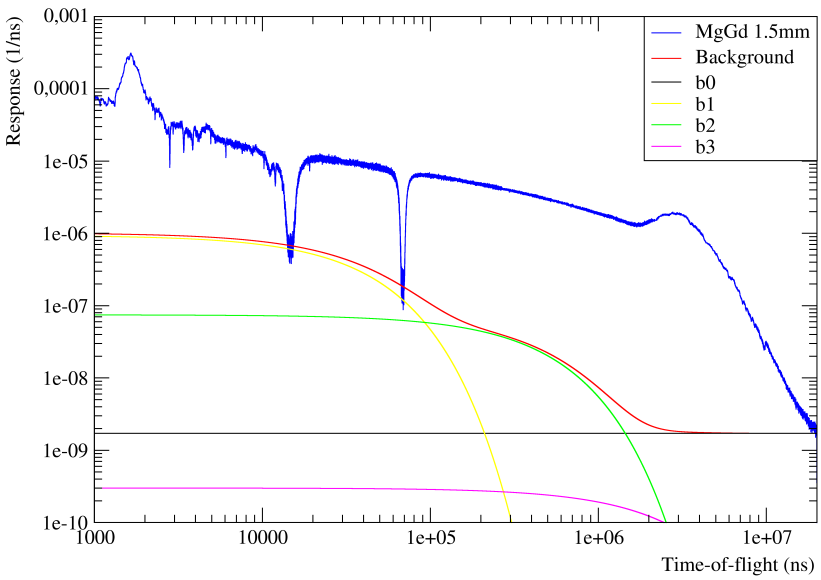

Figure 4.9: Time-of-flight spectrum with the 1.5mm MgGd alloy in the beam with Na and Co filters (blue) together with the total background (red). The different contribution to the background are also given.

Sample	b_0	b_1	λ_1	b_2	λ_2	b_3	λ_3	τ_0 (ms)
^{155}Gd Thin C_{in}	1.29×10^{-9}	1.00×10^{-6}	-3.00×10^{-5}	7.14×10^{-8}	-2.18×10^{-6}	1.91×10^{-6}	-5.27×10^{-7}	20
^{155}Gd Thin C_{out}	1.29×10^{-9}	1.06×10^{-6}	-3.00×10^{-5}	7.98×10^{-8}	-2.18×10^{-6}	2.36×10^{-6}	-4.26×10^{-7}	20
^{157}Gd Thin C_{in}	1.26×10^{-9}	9.47×10^{-7}	-3.00×10^{-5}	7.35×10^{-8}	-2.29×10^{-6}	1.53×10^{-6}	-5.96×10^{-7}	20
^{157}Gd Thin C_{out}	1.26×10^{-9}	9.24×10^{-7}	-3.00×10^{-5}	7.56×10^{-8}	-2.29×10^{-6}	2.26×10^{-6}	-4.30×10^{-7}	20
^{155}Gd Thick C_{in}	1.29×10^{-9}	1.09×10^{-6}	-2.40×10^{-5}	3.51×10^{-7}	-4.50×10^{-6}	9.44×10^{-8}	-5.31×10^{-7}	2.5
^{155}Gd Thick C_{out}	1.29×10^{-9}	1.08×10^{-6}	-2.40×10^{-5}	3.63×10^{-7}	-4.50×10^{-6}	9.47×10^{-8}	-5.31×10^{-7}	2.5
^{157}Gd Thick C_{in}	1.29×10^{-9}	1.07×10^{-6}	-2.40×10^{-5}	3.51×10^{-7}	-4.50×10^{-6}	9.23×10^{-8}	-5.28×10^{-7}	2.5
^{157}Gd Thick C_{out}	1.29×10^{-9}	1.07×10^{-6}	-2.40×10^{-5}	3.56×10^{-7}	-4.50×10^{-6}	9.27×10^{-8}	-5.29×10^{-7}	2.5
^{154}Gd C_{in}	7.84×10^{-9}	1.62×10^{-6}	-2.60×10^{-5}	1.28×10^{-7}	-3.00×10^{-6}	1.58×10^{-6}	-1.23×10^{-6}	2.5
^{154}Gd C_{out}	7.79×10^{-9}	1.58×10^{-6}	-2.60×10^{-5}	1.25×10^{-7}	-3.00×10^{-6}	1.67×10^{-6}	-1.25×10^{-6}	2.5
MgGd 0.8mm C_{in}	1.71×10^{-9}	7.42×10^{-7}	-3.00×10^{-5}	6.33×10^{-8}	-2.52×10^{-6}	1.93×10^{-6}	-4.40×10^{-7}	20
MgGd 0.8mm C_{out}	1.77×10^{-9}	7.71×10^{-7}	-3.00×10^{-5}	6.58×10^{-8}	-2.52×10^{-6}	1.93×10^{-6}	-4.28×10^{-7}	20
MgGd 1.5mm C_{in}	1.71×10^{-9}	9.37×10^{-7}	-3.00×10^{-5}	7.46×10^{-8}	-2.61×10^{-6}	2.29×10^{-6}	-4.47×10^{-7}	20
MgGd 1.5mm C_{out}	1.91×10^{-9}	9.67×10^{-7}	-3.00×10^{-5}	7.37×10^{-8}	-2.61×10^{-6}	2.38×10^{-6}	-4.30×10^{-7}	20
MgGd 2.0mm C_{in}	1.60×10^{-9}	1.07×10^{-6}	-3.00×10^{-5}	6.58×10^{-8}	-3.04×10^{-6}	2.41×10^{-6}	-4.54×10^{-7}	20
MgGd 2.0mm C_{out}	1.79×10^{-9}	1.03×10^{-6}	-3.00×10^{-5}	6.20×10^{-8}	-3.04×10^{-6}	2.47×10^{-6}	-4.30×10^{-7}	20
MgGd 3.0mm C_{in}	1.52×10^{-9}	9.25×10^{-7}	-3.00×10^{-5}	7.75×10^{-8}	-2.52×10^{-6}	2.18×10^{-6}	-4.64×10^{-7}	20
MgGd 3.0mm C_{out}	1.78×10^{-9}	9.51×10^{-7}	-3.00×10^{-5}	7.72×10^{-8}	-2.52×10^{-6}	2.30×10^{-6}	-4.28×10^{-7}	20

Table 4.1: Parameters for the analytical expression of the background for all the different measurements.

4.4 R-Matrix formalism

The resolved resonance region can be described by the R-Matrix theory. In this theory, all the reactions are considered as binary. The notation used in the description of the R-Matrix theory will be that of Lane and Thomas [41]. In a nuclear reaction, each channel is fully specified by:

- α, the partition of the compound system into reaction partners e.g. ^{155}Gd+n or ^{156}Gd+γ (both involving the same compound nucleus);
- **J,** the total angular momentum in units of $\hbar$;
- l, the orbital angular momentum in unit of $\hbar$;
- **s,** the channel spin in units of $\hbar$, defined as $\vec{s} = \vec{i} + \vec{I}$.

where for neutron-induced reactions $\vec{\mathbf{J}} = \vec{I} + \vec{l} + \vec{i}$ where $\vec{I}$ is the nucleus spin, $\vec{l}$ is the neutron orbital angular momentum and $\vec{i}$ is the neutron spin. The so-called statistical spin factor g:

$$g = \frac{2J+1}{(2i+1)(2I+1)}, \tag{4.5}$$

is the weight for the various possible total angular momentum J and it is related to the probability of obtaining the total angular momentum J from the intrinsic spins of the nucleon I and neutron i. For both ^{155}Gd and ^{157}Gd the ground state is $J^\pi = \frac{3}{2}^+$ so for s-wave neutrons the only available total angular momenta are 1^+ or 2^+.

The partial neutron cross section $\sigma_{cc'}$ for a given ingoing wave in channel c leading to an outgoing wave in channel c' is given by:

$$\sigma_{cc'} = \pi\lambda^2 g|\delta_{cc'} - U_{cc'}|^2 \tag{4.6}$$

where $U_{cc'} = U^J_{\alpha ls,\alpha' l' s'}$ is the collision matrix and therefore $|U_{cc'}|^2$ is the probability of a transition from channel c to channel c'. The elastic cross section can be expressed as:

$$\sigma_{\alpha\alpha} = \pi\lambda^2 \sum_J g \sum_{l,s} (|1 - U_{cc}|^2 + \sum_{l',s' \neq l,s} |U_{cc'}|^2) \tag{4.7}$$

While the reaction cross section for $\alpha \neq \alpha'$ depends quadratically on $U_{cc'}$:

$$\sigma_{\alpha\alpha'} = \pi\lambda \sum_J g \sum_{l',s'} |U_{cc'}|^2 \tag{4.8}$$

the total cross section is a linear function of $U_{cc'}$

$$\sigma_\alpha = 2\pi\lambda^2 \sum_J g \sum_{l,s} (1 - \Re(U_{cc})). \tag{4.9}$$

The R-matrix theory allows us to express U_{cc} in terms of the channel matrix R:

$$U_{cc'} = e^{-i(\varphi_c + \varphi_{c'})}\{\delta_{cc'} + 2iP^{1/2}[(1 - RL^o)^{-1}R]_{cc'}P_{c'}^{1/2}\} \tag{4.10}$$

$$R_{cc'} = \sum_r \frac{\gamma_{rc}\gamma'_{rc}}{E_r - E} \tag{4.11}$$

$$L^o_{cc'} = (S_c + iP_c - B_c)\delta_{cc'} \tag{4.12}$$

where:

1. $R_{cc'}$ is the R-matrix element;
2. φ_c is the hard-sphere scattering phase shift
3. S_c is called shift factor and is the real part of the logarithmic derivative of the outgoing wave function at channel radius a;
4. P_c is the centrifugal barrier penetrabilities and is the imaginary part of the logarithmic derivative of the outgoing wave function at the channel radius a;
5. B_c is the logarithmic derivative of the radial eigenfunctions at channel radius a;
6. $\gamma_{rc}(\gamma_{rc'})$ is the probability of the formation(decay) of the compound state via channel c(c');
7. E_r is the resonance energy.

In the R-matrix theory, the γ_{rc} have a normal distribution and they are related to the resonance width via the equation:

$$\Gamma_{rc} = 2\gamma_{rc}^2 P_c. \tag{4.13}$$

4.4.1 Single Level Breit-Wigner approximation

Before the R-Matrix theory was introduced, the Single Level Breit-Wigner (SLBW) formulas were used to parametrize cross section data. The Breit-Wigner formula can be seen as an approximation of the R-Matrix theory and, for isolate resonances that are not affected by multi-level interferences, it provides accurate results. In the Single Level Breit-Wigner approximation, if we suppose that only elastic scattering and capture may occur, the scattering and capture cross section are expressed as:

$$\sigma_n = 4\pi g R'^2 + 4\pi\lambda^2 \frac{g\Gamma_n^2}{4(E-E_r)^2+\Gamma^2} + 16\pi\lambda R \frac{g\Gamma_n(E-E_r)}{4(E-E_r)^2+\Gamma^2} \tag{4.14}$$

$$\sigma_\gamma = 4\pi\lambda^2 \frac{g\Gamma_n\Gamma_\gamma}{4(E-E_r)^2+\Gamma^2} \tag{4.15}$$

The scattering cross section is, therefore, a sum of three terms:

1. a constant potential scattering cross section;
2. a symmetric resonance term;
3. an asymmetric resonance term which is given by the interference between potential and resonance.

4.5 Analysis of the experimental data

For a non-fissile nucleus, the total and reaction cross section can be parametrized using resonance parameters such as potential scattering radius, resonance energy, partial widths, spin, and parity of the resonance. A full set of parameters can be determined by a combination of different measurements such as:

1. transmission
2. radiative capture
3. self-indication

Transmission is the percentage of neutrons that traverses a sample without interacting with it, radiative capture is the percentage of neutrons that undergoes capture reaction while self-indication is performed measuring the transmission of a filter sample using a reaction in a second sample placed downstream.

To extrapolate those parameters from the data a complete Resonance Shape Analysis (RSA) of the data must be performed. However, in order to obtain good results from the analysis some experimental effects, such as Doppler broadening and the resolution function of the spectrometer must be studied.

4.5.1 Doppler Broadening

In the measurements, the resonance shape is not exactly the Breit-Wigner one but is broadened because of the thermal motion of nuclei inside the sample. This effect is known as Doppler broadening. Using the ideal gas approximation, which is approximating the nuclei inside the sample as a free gas at the temperature T, one can obtain the Doppler broadened cross section with a convolution of the not broadened cross section and a Gaussian with a FWHM given by $2\sqrt{2}\Delta$. This Δ is the experimental Doppler width and it is defined as:

$$\Delta = \sqrt{\frac{4EkT}{M/m}} \tag{4.16}$$

where k is the Boltzmann constant, M the nucleus mass and m the incident particle mass. Δ gives a measure of the observed broadening in resonances. This effect is more important at higher energies and can limit the resolution on the width.

4.5.2 Resolution function

Another source of the broadening of the shape of resonances is the experimental resolution. The energy of the incident neutron it is not exactly known. The truly observed yield in a time-of-flight measurement is:

$$\bar{Y_x}(E) = \int dE' r(E', E) Y_x(E) \tag{4.17}$$

where $dE'r(E', E)$ is the probability that an event observed at the energy E was actually due to a beam particle with an energy E' in dE'. In first approximation, the resolution function can be taken as Gaussian:

$$r(E', E) = \frac{1}{W\sqrt{\pi}} e^{-(E'-E)^2/W^2} \tag{4.18}$$

where W depends on the following parameters:

1. finite accelerator burst width (t_b)
2. finite time channel width (t_c)
3. electronic drift, jitter (t_d)
4. uncertain starting (moderator) and ending point (sample) of the flight base (ΔL)
5. angular resolution ($\Delta\theta$)

For a more accurate study, the resolution function is also estimated using Monte Carlo simulation.

Chapter 5

Results

In this chapter, the results obtained in the experimental campaign are reported. First of all, I show a comparison between the data obtained in the present measurements with the data of the libraries. After this, I illustrate the resonance shape analysis of the experimental data. In particular, I present the procedure for the normalization of the transmission data, the fit of the thermal resonances of both ^{155}Gd and ^{157}Gd, and the analysis performed on some of the lower energy resonances for ^{154,155,157}Gd samples. More specifically, the data obtained with the ^{154}Gd were used to check the consistency of the isotopic composition of the sample and the agreement of the resonance observed with ^{155,157}Gd thick samples. Lastly, I discuss the necessity of a new experimental campaign using very thick natural gadolinium to accurately determine the isotopic composition of the enriched samples.

5.1 Comparison with libraries

After the data reduction, the transmission spectra for all the measured samples were obtained. These spectra were compared to the ones obtained using the resonance parameters from the ENDF/B-VIII library and all the sample information listed in the previous chapter. In Fig.5.1, Fig.5.2 and Fig.5.3 the comparison of ^{155}Gd, ^{157}Gd and ^{154}Gd enriched samples is shown respectively. In Fig.5.4 the MgGd data are illustrated.

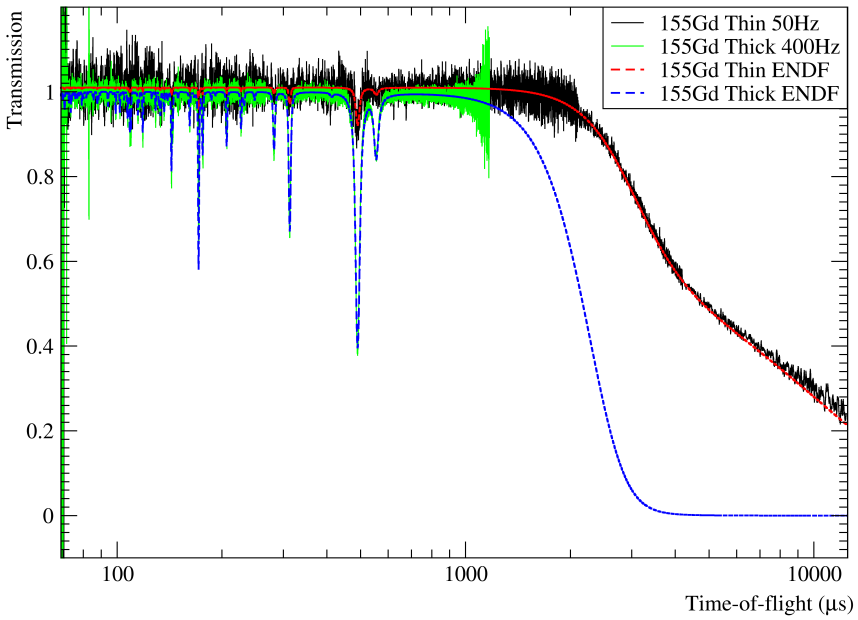

Figure 5.1: Comparison between experimental data and ENDF/B-VIII library for thin and thick ^{155}Gd enriched samples.

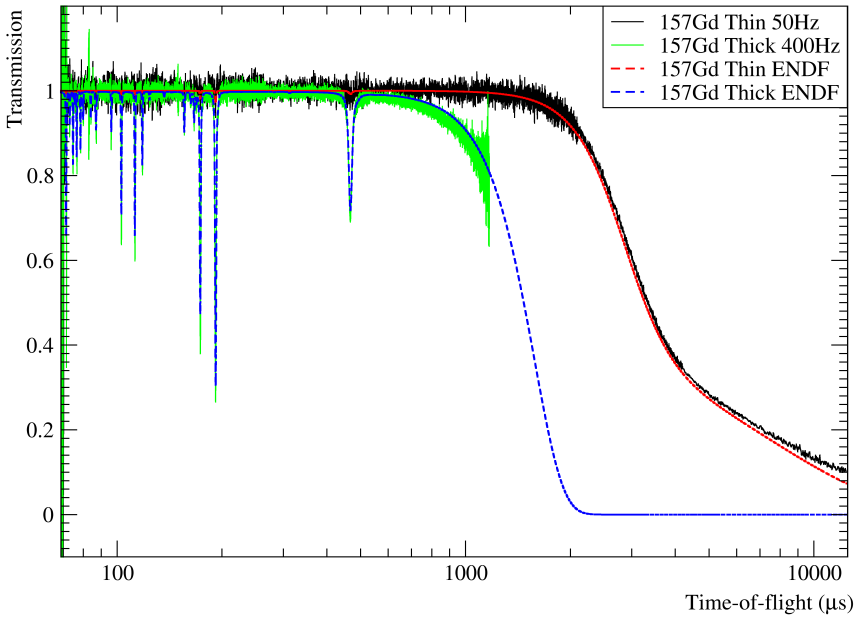

Figure 5.2: Comparison between experimental data and ENDF/B-VIII library for thin and thick ^{157}Gd enriched samples.

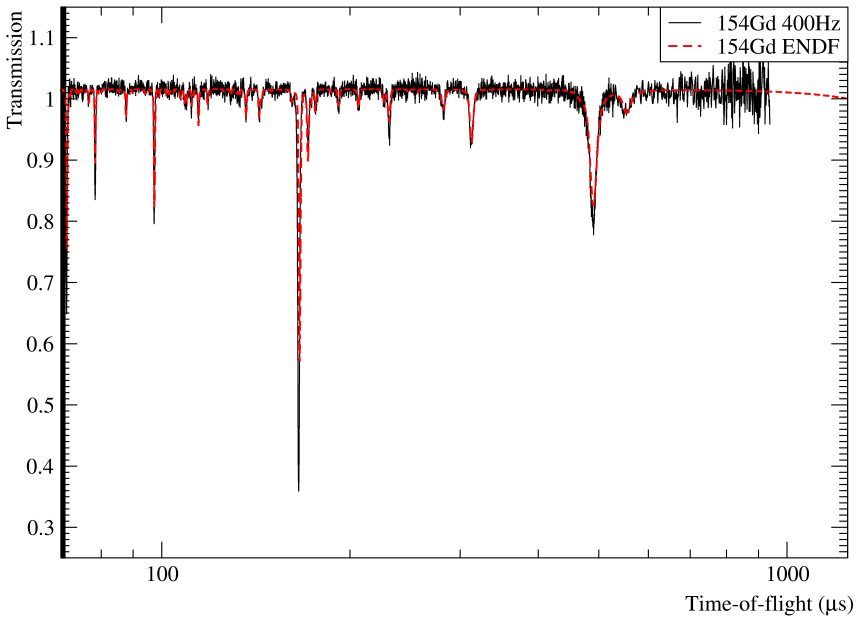

Figure 5.3: Comparison between experimental data and ENDF/B-VIII library data for ^{154}Gd enriched samples.

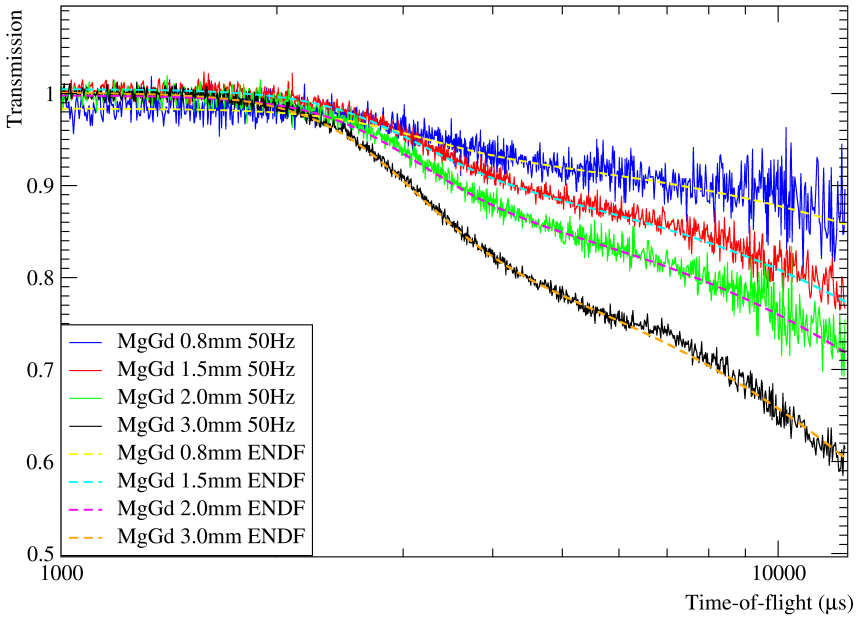

Figure 5.4: Comparison between experimental data and ENDF/B-VIII library for MgGd alloys.

In Fig.5.1 and Fig.5.2 we can notice a small deviation in the thermal transmission for both ^{155}Gd and ^{157}Gd thin samples. In fact, the observed transmission is higher than the one obtained with the ENDF/B-VIII data for both isotopes. This suggests an overestimation of the thermal cross section for both the odd isotopes in the ENDF library. A magnification of this region together with the residuals (defined as $\frac{T_{exp}-T_{ENDF}}{\sigma}$) are shown in Fig.5.5 and Fig.5.6 for ^{155}Gd and ^{157}Gd respectively. Here we can see how the difference for ^{157}Gd is non-negligible. Looking at higher energies we can notice a good agreement of the observed resonances with the data in the library. We can also notice how the resonances are visible only in the thick samples.

In Fig.5.3 we can see an overall good agreement of the experimental data with the ENDF/B-VIII library. We can notice a deviation in the two bigger resonances at 2.5 and 22.9 eV (493 and 166 μs respectively). In particular the 2.5 eV resonance is a ^{155}Gd resonance visible also in Fig.5.1.

From Fig.5.4 we can see the four MgGd alloys measured and calculated transmission. As we can see there is a good agreement of the experimental data with the ENDF library in the thermal region. At higher energy, the transmission is constant because the samples are too thin to observe any gadolinium resonance. A small deviation of the data from the calculated transmission can be seen for the 3.0 mm sample at around 7000 μs.

5.2 REFIT Fit

After the data reduction, the obtained transmission data were analysed using the R-Matrix program REFIT [2]. REFIT has been developed to overcome some of the problems associated with the single-level resonance formalism using the R-Matrix formalism. This program was also used to produce the previously showed images to include in the theoretical calculation all the experimental effects (e.g. Doppler broadening, resolution function, etc.). The first step of the analysis was the determination of the normalization factors for all the transmission spectra.

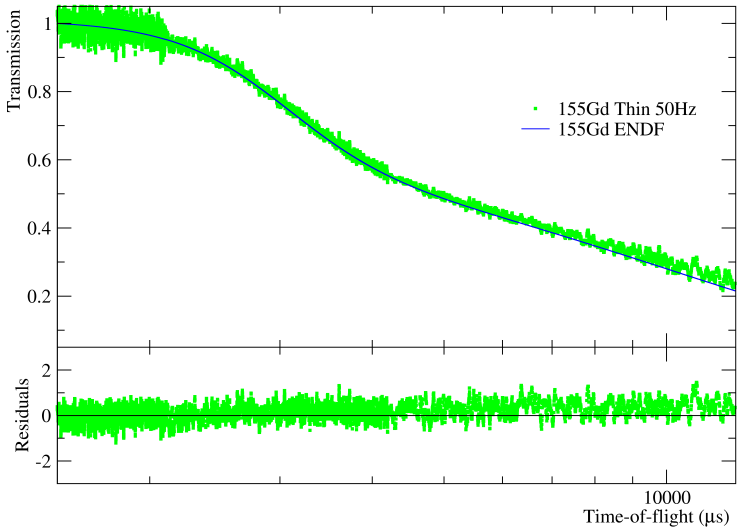

Figure 5.5: Magnification of the low-energy region of TOF spectra for ^{155}Gd thin sample at 50Hz (up green), theoretical transmission based on ENDF data (up blue) and residuals (bottom panel).

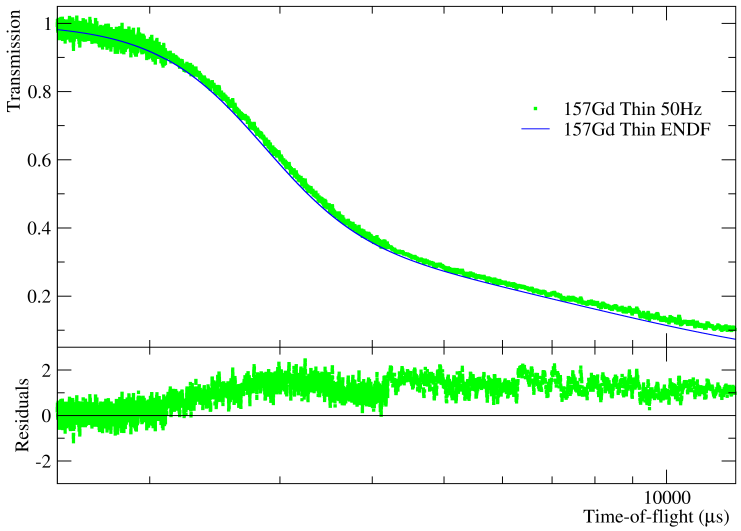

Figure 5.6: Magnification of the low-energy region of TOF spectra for ^{157}Gd thin sample at 50Hz (up green), theoretical transmission based on ENDF data (up blue) and residuals (bottom panel).

5.2.1 Normalization factors

The normalization of the transmission is a time-independent factor that multiplies all the spectrum. In this way is possible to correct experimental effects that cause a shift in the transmission making it different from unity in regions where the sample is transparent to the neutron beam. The normalization factor was estimated fitting one or more flat regions of the experimental spectra. All the measured normalization factors slightly differ from one, on average we have a deviation of 0.3%. The only exception to this behaviour is the 0.8 mm MgGd alloy. In fact, for this sample, the transmission was measured as the ratio of sample-in and open beam without any dummy. Thanks to the small thermal cross section of magnesium and the fact that it does not change a lot with the neutron energy, it was possible to correct the effect of magnesium in the thermal region using the normalization factor. In Fig.5.7 are shown the experimental transmission of the 0.8 mm MgGd alloy (black) together with the non-normalized theoretical transmission (red) and the normalized one (green). In Tab.5.1 a list of all the normalization factors is reported.

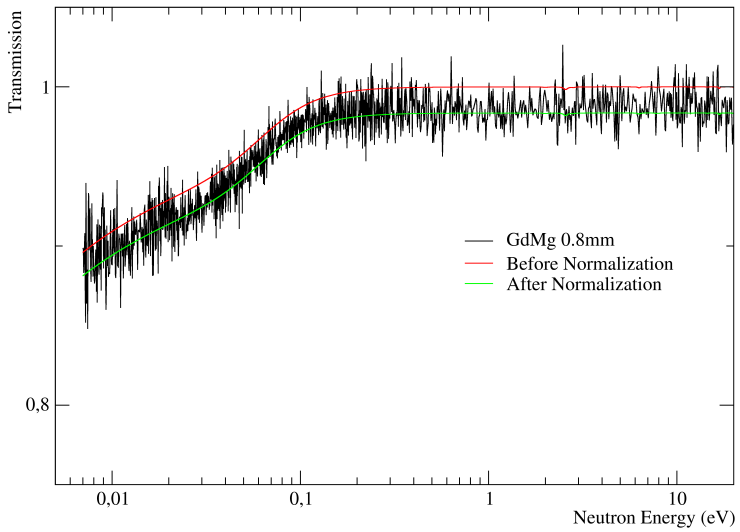

Figure 5.7: Transmission spectrum of the 0.8 mm MgGd alloy (black), non-normalized theoretical transmission (red) and normalized theoretical transmission (green) as a function of the neutron energy.

Sample	Normalization
^{155}Gd Thin	0.990
^{155}Gd Thick	0.999
^{157}Gd Thin	1.000
^{157}Gd Thick	1.005
^{154}Gd	0.984
MgGd 0.8 mm	1.017
MgGd 1.5 mm	0.995
MgGd 2.0 mm	1.002
MgGd 3.0 mm	0.999

Table 5.1: Normalization factors measured for all the analysed samples.

5.2.2 Near-Thermal resonances fit

After the estimation of the normalization parameters, it was possible to perform the resonance shape analysis. The first two resonances that were analysed were the thermal resonances of ^{155,157}Gd. These resonances, especially the ^{157}Gd one, are the main responsible for the big thermal cross section of natural gadolinium. Using REFIT it was possible to fit the resonance parameters $(E_n, \Gamma_\gamma, \Gamma_n)$ of these two resonances. In this fit, the spin of the resonance was fixed to the value existing in the libraries and the neutrons were all supposed in s-wave (angular momentum = 0). In Fig.5.8 and Fig.5.9 the transmission measured with ^{155}Gd and ^{157}Gd thin samples together with the result of the fit and the residuals are shown respectively in the energy region below 1 eV. The transmission is shown as a function of the neutron energy. As we can see from the figures, the fitted parameters reproduce perfectly the shape of the data. Also, the position of the knee (the region of the transmission spectra where the thermal resonances start to play an important role) are well reproduced with these new parameters.

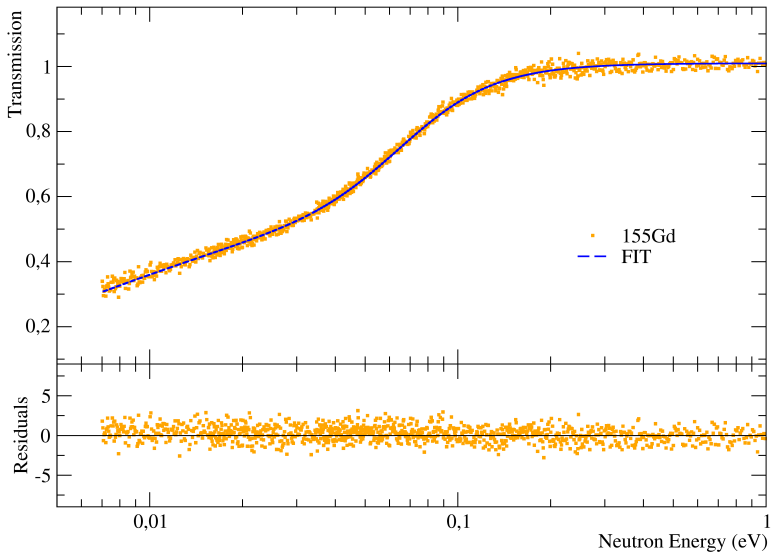

Figure 5.8: Experimental transmission of ^{155}Gd thin samples in the energy region below 1 eV (orange) and best fit of these data obtained with REFIT (blue).

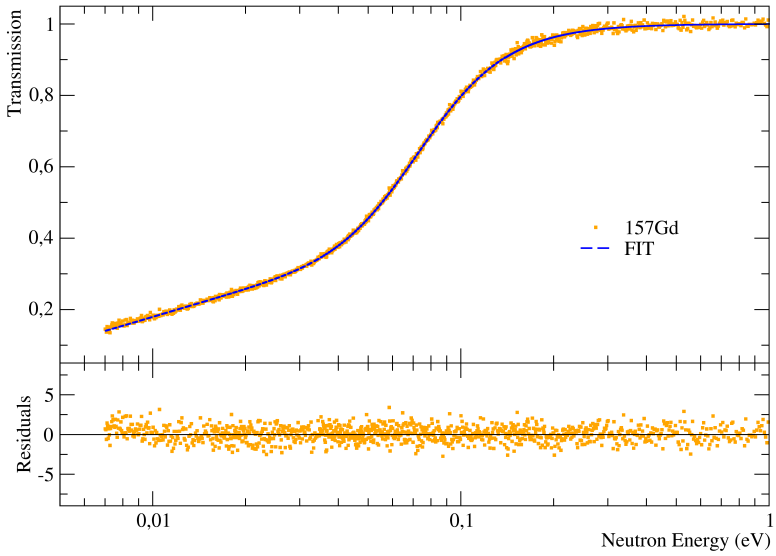

Figure 5.9: Experimental transmission of ^{157}Gd thin samples in the energy region below 1 eV (orange) and best fit of these data obtained with REFIT (blue).

It is also very interesting to compare the results of this fit with the resonance parameters obtained by the n_TOF measurements [1]. In fact, the same enriched samples were used in this capture experiment. The comparisons of the experimental data of both samples with the resonance parameters obtained with the fit (blue) and the theoretical transmission obtained using the n_TOF resonance parameters (green) are shown in Fig.5.10 and Fig.5.11 for ^{155}Gd and ^{157}Gd samples respectively. As we can notice from these figures the results of these two experiments are very similar. For ^{155}Gd we have a small deviation in the low-energy region of the spectrum. In this region, we can see that the transmission obtained using the n_TOF parameters is slightly lower than the one obtained with the fit. For ^{157}Gd we have a little difference in the shape of the resonance probably caused by a small energy shift in the resonance parameters. The obtained parameters E_n, Γ_γ, and Γ_n are reported with their uncertainties in Tab.5.2.

Sample	E_n (eV)	Γ_γ (meV)	Γ_n (meV)
^{155}Gd	0.0274 (2)	106.1 (6)	0.1017 (5)
^{157}Gd	0.03145 (5)	100.9 (2)	0.4328 (8)

Table 5.2: Resonance parameters of the ^{155}Gd and ^{157}Gd thermal resonances fitted from the data using REFIT.

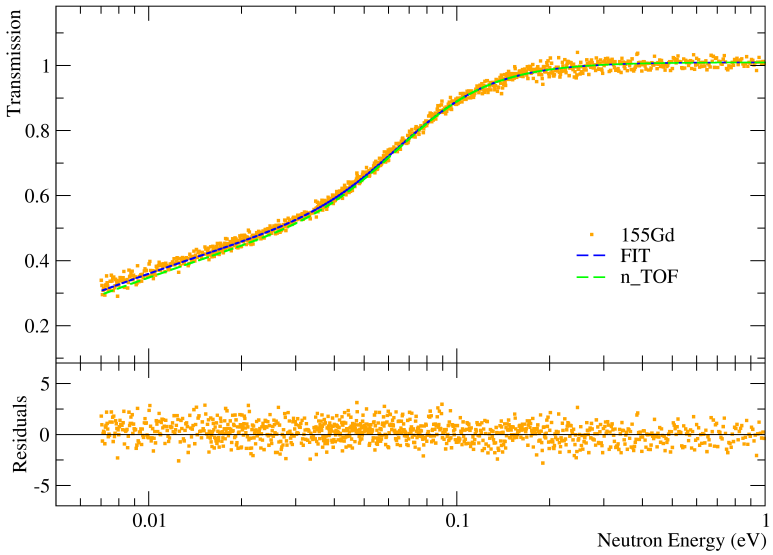

Figure 5.10: Experimental transmission of ^{155}Gd thin samples in the energy region below 1 eV (orange) compared with the best fit of these data obtained with REFIT (blue) and transmission calculated with n_TOF resonance parameters.

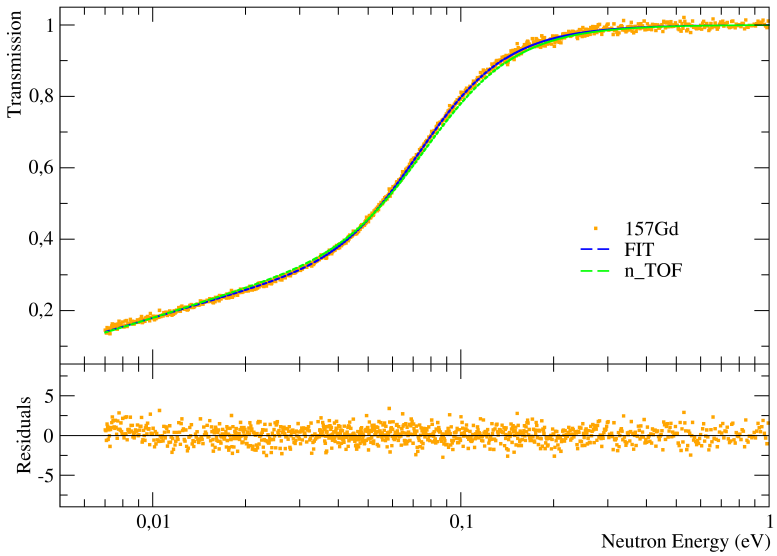

Figure 5.11: Experimental transmission of ^{155}Gd thin samples in the energy region below 1 eV (orange) compared with the best fit of these data obtained with REFIT (blue) and transmission calculated with n_TOF resonance parameters.

5.2.3 MgGd alloys comparison

After fitting the resonance parameters of the near-thermal resonances of ^{155,157}Gd it was possible to obtain a new estimation of natural gadolinium transmission. Using the areal densities of the four MgGd alloys, obtained via mass and area measurement performed at the JRC, the transmission was calculated for all the samples. A comparison of this calculation with the experimental data was then performed to assess the compatibility of the different sets of data. The comparisons are shown in Fig.5.12, Fig.5.13, Fig.5.14, and Fig.5.15 for 0.8 mm, 1.5 mm, 2.0 mm, and 3.0 mm samples respectively.

As we can see from these plots we have a very good agreement of the R-Matrix calculation with the experimental data. For all the samples the region of the knee, which is between 0.09 eV and 0.2 eV, is well reproduced. The calculation can correctly reproduce all the measured transmissions below 1 eV for all the samples with residuals between -3 and 3 in the entire energy range. The only exception to this behaviour can be seen in the 3.0 mm sample. Looking at the region between 10 and 30 meV we can see a structure in the transmission. This kind of structure can not be explained by modifying the resonance parameters of gadolinium and therefore a further investigation is required. A capture measurement on the same sample performed this year at the JRC can be used to further analyse this behaviour.

It is also possible to compare the agreement of these transmission data with the information in different libraries. The main libraries for nuclear data are ENDF/B-VIII, JEFF-3.3 and JENDL-4.0 which are respectively United States, Europe and Japan nuclear data library. A comparison of the data with all these libraries and with the calculation based on the fit of enriched samples is shown in Fig.5.16. As we can see, the transmission obtained with JENDL and ENDF is lower than the measured one for all the sample and the deviation became more and more visible with the thickness of the alloy. On the other hand, JENDL transmission is higher for all the samples. We can notice how the transmission calculated with the fitted parameters reproduces more accurately the data for all thicknesses. Moreover, neither the libraries can reproduce the structure observed in the 3.0 mm sample.

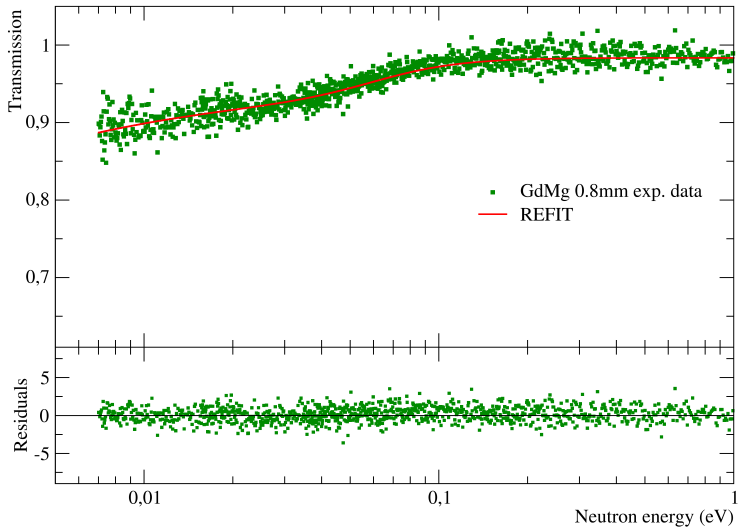

Figure 5.12: In the upper panel comparison of the experimental transmission of the 0.8 mm MgGd alloy (green) and the theoretical calculation obtained with the fit of ^{155,157}Gd thermal resonances (red) is shown. The residuals are shown in the bottom panel.

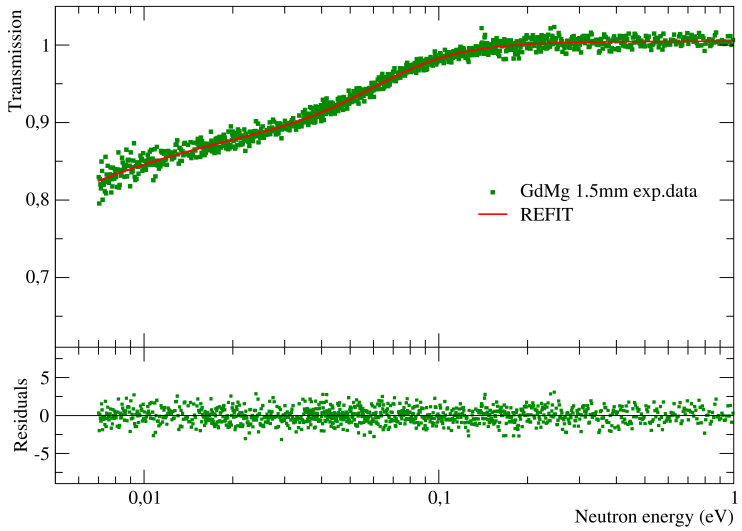

Figure 5.13: In the upper panel comparison of the experimental transmission of the 1.5 mm MgGd alloy (green) and the theoretical calculation obtained with the fit of ^{155,157}Gd thermal resonances (red) is shown. The residuals are shown in the bottom panel.

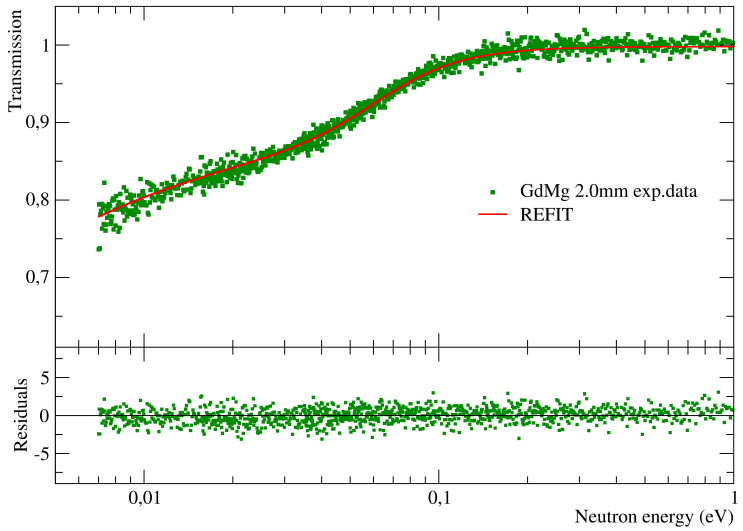

Figure 5.14: In the upper panel comparison of the experimental transmission of the 2.0 mm MgGd alloy (green) and the theoretical calculation obtained with the fit of ^{155,157}Gd thermal resonances (red) is shown. The residuals are shown in the bottom panel.

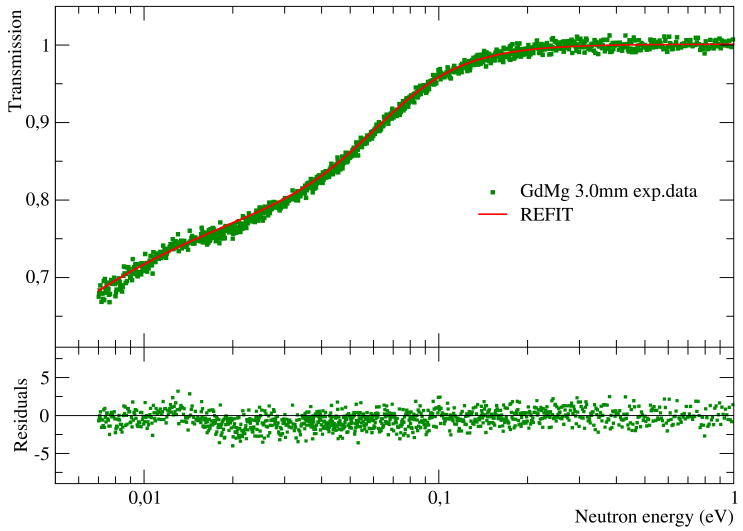

Figure 5.15: In the upper panel comparison of the experimental transmission of the 3.0 mm MgGd alloy (green) and the theoretical calculation obtained with the fit of ^{155,157}Gd thermal resonances (red) is shown. The residuals are shown in the bottom panel.

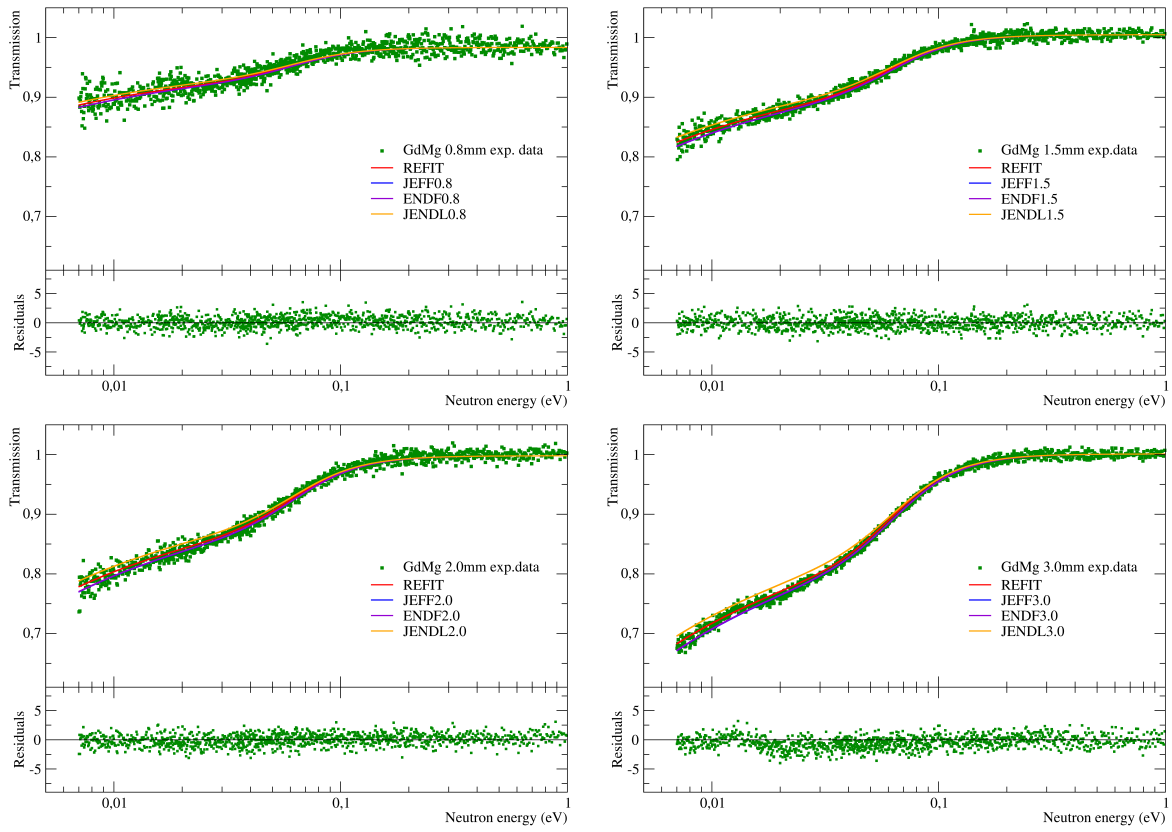

Figure 5.16: Comparison of the transmission data obtained with MgGd alloys (green) with JEFF (blue), ENDF (purple), JENDL (orange) and the calculation obtained with the fitted parameters (red). Top left 0.8 mm, top right 1.5 mm, bottom left 2.0 mm, bottom right 3.0 mm sample.

5.2.4 Thermal capture cross section

After the fit of the thermal resonances of both ^{155,157}Gd, it was possible to obtain the capture cross section of these isotopes at thermal energy. To obtain the cross section relative to one specific isotope, it was necessary to change the macro used with REFIT. In fact, the used samples contained more than one isotope and the cross section obtained directly with these samples was the total cross section of the sample, not the one relative to pure ^{155,157}Gd. A couple of dummy samples made of pure ^{155}Gd or ^{157}Gd were inserted in the macro. These dummies had a thickness equal to the real thickness of the enriched sample multiplied by the real isotopic composition. Using these dummy samples together with the new resonance parameters obtained for the odd isotopes it was possible to obtain the capture cross section of ^{155,157}Gd. The capture cross section spectra for both isotopes are shown in Fig.5.17. The total uncertainties were obtained taking into account the effects of the uncertainties given by the normalization factor, the signal-to-noise ratio and the counting statistics. The error of the normalization factor is 0.25% as shown in the previous chapter (see Section 4.2.1). The signal-to-noise ratio was obtained directly from the time-of-flight spectra of sample-in and sample-out configuration for both ^{155}Gd and ^{157}Gd. The measured uncertainties given by the signal-to-noise ratio were 0.46% and 0.78% for ^{155}Gd and ^{157}Gd respectively. The uncertainties given by the counting statistic were obtained directly from the fitted parameters. The $\Delta\sigma/\sigma$ due to counting statistics obtained with this procedure were 0.24% and 0.18% for ^{155}Gd and ^{157}Gd respectively. The total uncertainties given by these three values are 0.58% and 0.84% for ^{155}Gd and ^{157}Gd respectively. The calculated thermal capture cross sections with their total uncertainties are shown in Tab.5.3.

	^{155}Gd	^{157}Gd
σ_0 (kb)	59.7(3)	244(2)

Table 5.3: Thermal capture cross section measured for ^{155,157}Gd using fitted resonance parameters.

As we can see, the ^{155}Gd is slightly lower than the value in the ENDF library (60.89 kb). Also, the ^{157}Gd one is slightly lower than the ENDF value (253.32 kb). Looking at the previous evaluation of these values we can notice that the value obtained for ^{155}Gd is very close to all the previous results, except for a difference with Choi's result (56.7 kb). For ^{157}Gd our evaluation has a big disagreement with Leinweber's result (226 kb) while it is compatible with the n_TOF measurement (239.8(9.3) kb). A comparison between the cross sections measured in this experiment whit the n_TOF cross sections are shown in Fig.5.18

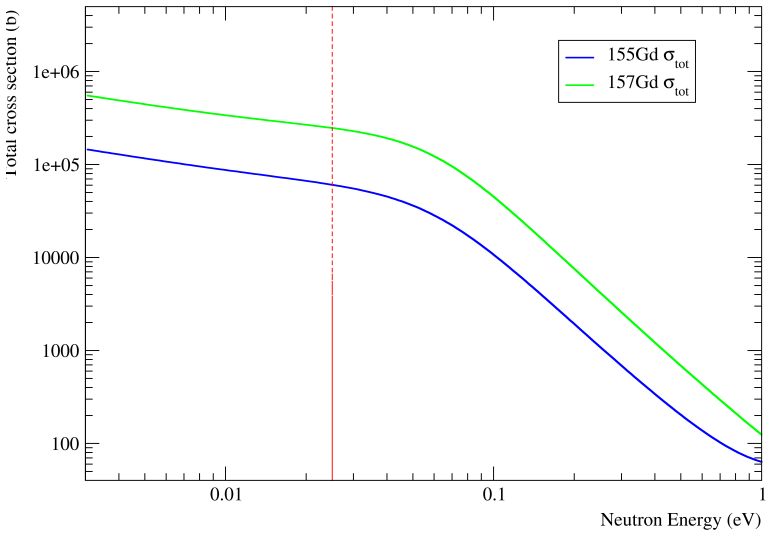

Figure 5.17: Total cross section of ^{155}Gd (blue) and ^{157}Gd (green) obtained using fitted parameters of thermal resonances. The red line is the thermal energy.

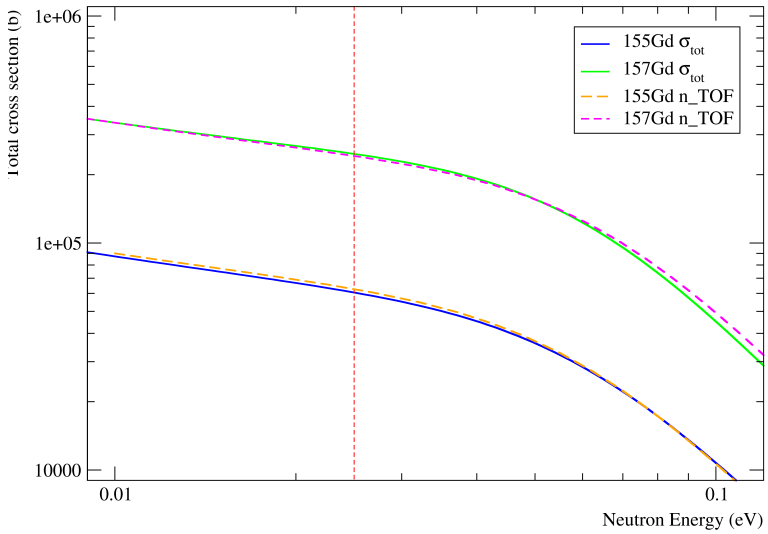

Figure 5.18: Comparison of the fitted cross section for ^{155}Gd (blue) and ^{157}Gd with the one obtained at n_TOF by Mastromarco and collaborators (magenta and orange respectively). The red line is the thermal energy.

5.2.5 Resonance Shape Analysis

Using the data obtained with ^{155,157}Gd thick samples it was possible to perform a Resonance Shape Analysis on some of the resonances. For both isotopes, the region of interest was the energy range below 100 eV. However, not all the resonances were analysed. For this analysis, only the resonances with a transmission lower than 0.9 were considered. Moreover, only resonances with a substantial deviation from the libraries were analysed. Using all these constraints, a total of seven resonances were analysed for ^{155}Gd while five resonances were studied for ^{157}Gd. The analysis was performed in a single run for all the parameters (E_n, Γ_γ, and Γ_n). A comparison between the experimental data (orange), data in ENDF library (green), and fitted values (red) is shown in Fig.5.19 and Fig.5.20 for ^{155}Gd and ^{157}Gd respectively. In Tab.5.4 all the results of the fit are shown.

^{155}Gd		
E_n (eV)	Γ_γ (meV)	$2g\Gamma_n$ (meV)
2.012(8)	115(2)	0.277(3)
2.5716(2)	101.2(4)	2.086(5)
6.3064(7)	106(2)	2.62(2)
7.749(2)	102(6)	1.37(3)
14.471(3)	99(10)	2.29(9)
19.865(4)	100(11)	5.4(2)
20.972(2)	113(5)	15.5(2)

^{157}Gd		
E_n (eV)	Γ_γ (meV)	$2g\Gamma_n$ (meV)
2.8282(4)	101(1)	0.472(3)
16.7820(6)	85(2)	17.81(8)
20.5120(8)	80(2)	17.14(9)
44.094(6)	67(17)	11.9(4)
48.665(3)	69(8)	34.9(5)

Table 5.4: Results of the Resonance Shape Analysis on ^{155}Gd thick sample (left) and ^{157}Gd thick sample (right).

As we can see the fitted parameters reproduces accurately all the analysed resonances. On the other hand, the residuals of the ENDF library show a poor agreement, especially on some resonances. We can notice for example the deviation at the 20.9 eV resonance of ^{155}Gd or the 16.8 eV and 20.5 eV resonances of ^{157}Gd where we have a residual higher

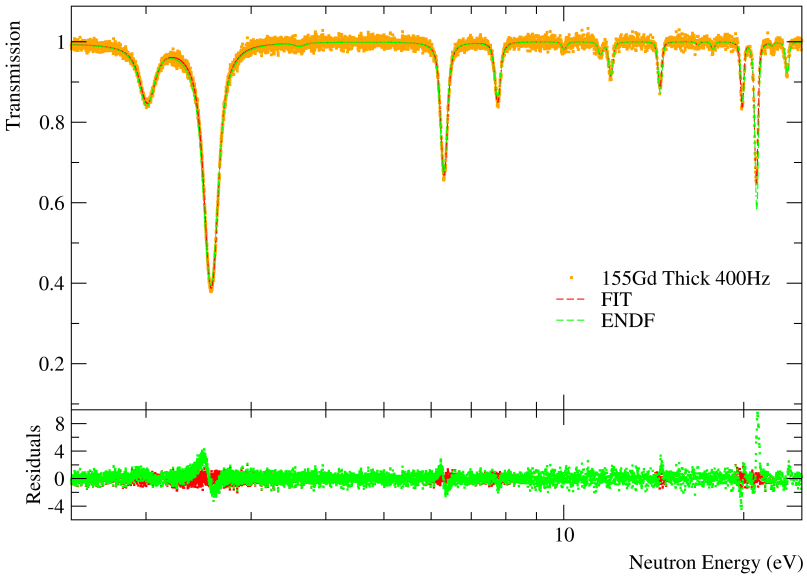

Figure 5.19: Comparison between the experimental data (orange), data in ENDF library (green), and fitted values (red) for the Resonance Shape Analysis of ^{155}Gd.

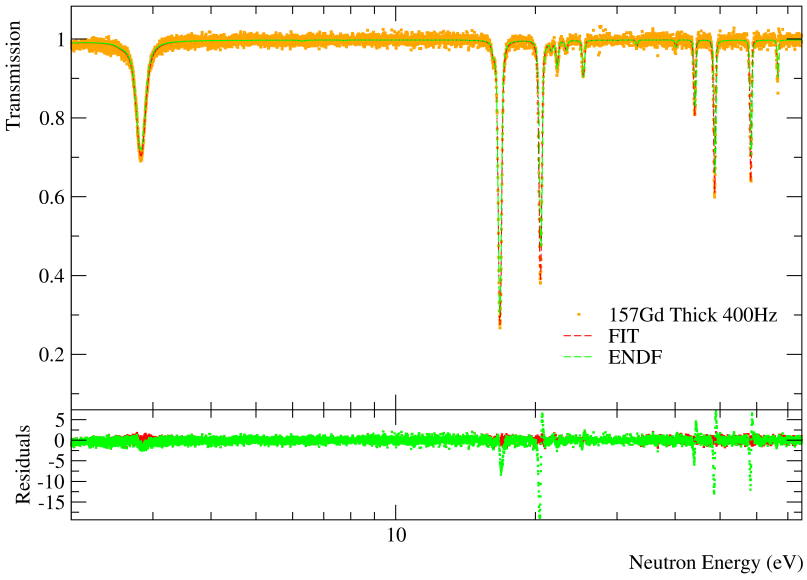

Figure 5.20: Comparison between the experimental data (orange), data in ENDF library (green), and fitted values (red) for the Resonance Shape Analysis of ^{157}Gd.

than 10 (in absolute value). In the 2.5 eV and 6.3 eV resonances of ^{155}Gd, we can observe an energy shift with respect to the ENDF library. An overall good agreement can be seen for smaller resonances not fitted in this work.

Looking at the results, we can notice a big difference between the capture width observed in this experiment and the one in literature for the last resonances of ^{157}Gd. In fact, the results of the fit suggest a radiation width lower than the one in the ENDF library. Looking at the 44.1 and 48.6 eV resonances, we obtained a radiation width of 67 and 69 respectively while in literature the values of the Γ_γ are 96 an 90 respectively.

Although these values allow us to reproduces faithfully the observed resonances, the great difference with the libraries and other measurements (e.g. n_TOF one, where we have values compatible with ENDF) together with uncertainty up to 25% make necessary a further investigation on these widths. This difference in the obtained radiation width and the big uncertainties are probably related to the little sensitivity of transmission measurement on these widths. A comparison of the parameters with a set of capture data can reduce the uncertainty on the Γ_γ.

As a comparison, we can observe the ratio between the kernel obtained in this work and the one measured at n_TOF. This ratio is showed in Fig.5.21 and 5.22 for ^{155}Gd and ^{157}Gd respectively. As we can notice from these figures, the ratio of the kernels is always compatible with one. The deviation from unity is below 9% for all the resonances of both isotopes. For many resonances, the errors on the kernel ratio are higher than 10%. This big uncertainty is caused by the low precision of Γ_γ in transmission measurements.

5.2.6 ^{154}Gd consistency

Using the information obtained in the previous analysis is possible to check the consistency of the transmission obtained with the ^{154}Gd enriched sample with these results. First of all, is possible to compare the nominal ^{155}Gd abundance with a fitted estimation. The isotopic abundance can be fitted with REFIT. The abundance was estimated using the three bigger resonances of ^{155}Gd (2.5 eV, 6.3 eV, and 20.9 eV) with the parameters fitted before with the ^{155}Gd thick sample. The resulting fitted abundance was 19.8(2)%

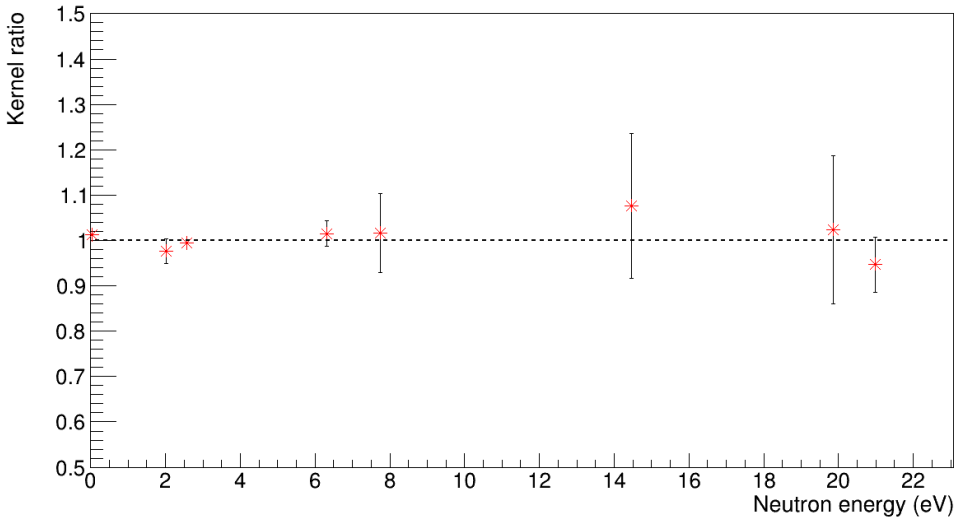

Figure 5.21: Ratio of the kernel measured at n_TOF by Mastromarco and collaborators [1] and the kernel obtained in this work for ^{155}Gd-thick enriched sample.

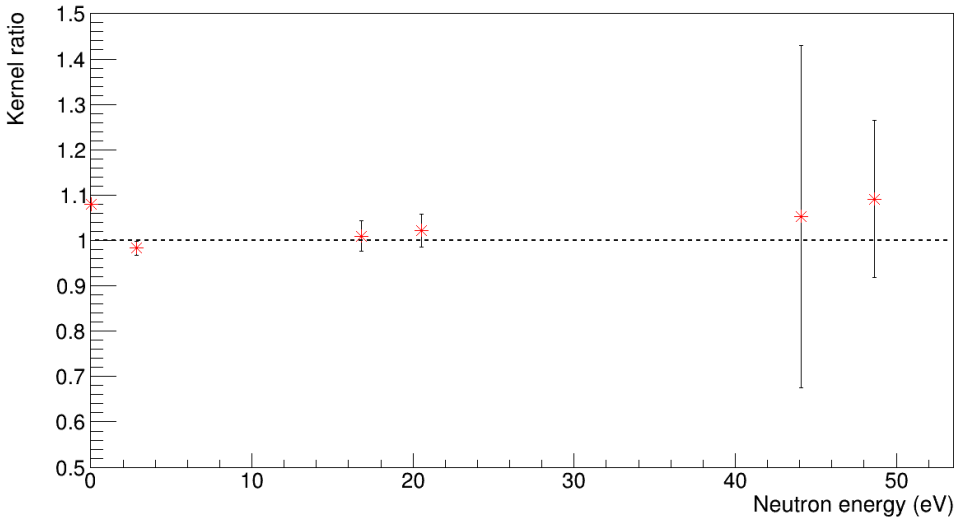

Figure 5.22: Ratio of the kernel measured at n_TOF by Mastromarco and collaborators [1] and the kernel obtained in this work for ^{157}Gd-thick enriched sample.

which is slightly higher than the one declared by the manufacturer (17.5(1)%). As we can notice these results are incompatible with each other. This incompatibility makes necessary a further investigation of the composition of this sample.

The abundance estimation of the other isotopes is not possible because there are no resonances big enough to be fitted. This fact is caused by the small abundance of the other isotopes ($> 8\%$ nominal abundance for ^{152,156,157,158,160}Gd) and by the thickness of the sample.

5.2.7 ^{nat}Gd additional measurements

In order to fully characterize the isotopical composition of enriched samples, a set of measurements with thick ^{nat}Gd samples can be used. In fact, for natural samples, the isotopical composition is known with very high precision. Therefore the information about resonances obtained with natural samples can be used to measure the isotopical composition of enriched samples. In 2015 a set of four natural gadolinium samples of different thicknesses was used at the JRC of Geel in a transmission experiment. Using the data obtained in these measurements, it is possible to perform a resonance shape analysis on the biggest resonances of all the gadolinium isotopes. In this way is possible to obtain the isotopical composition for all the stable isotopes of gadolinium. The thicker sample was a disk of 8 cm of diameter with a thickness of 0.2 mm. The areal density of the sample was 6.2865×10^{-4} atoms/b.

Looking at the resonance parameters in libraries for the different isotopes we can select a set of resonances that are isolated and big enough to be analysed. A list of these resonances is reported in Tab.5.5. As we can notice, only a single resonance is suitable for the analysis for ^{152,154}Gd. This results from the small abundance of these isotopes that make all the other resonances too small for the analysis.

In Fig5.23 the transmission spectrum obtained with the 0.2 mm ^{nat}Gd sample is shown. In the figure, we can see three different regions of the spectrum each one centred at one resonance. In particular, top left the 8.00 eV resonance of ^{152}Gd, top right the 65.06 eV resonance of ^{154}Gd and bottom the 904.90 eV resonance of ^{160}Gd.

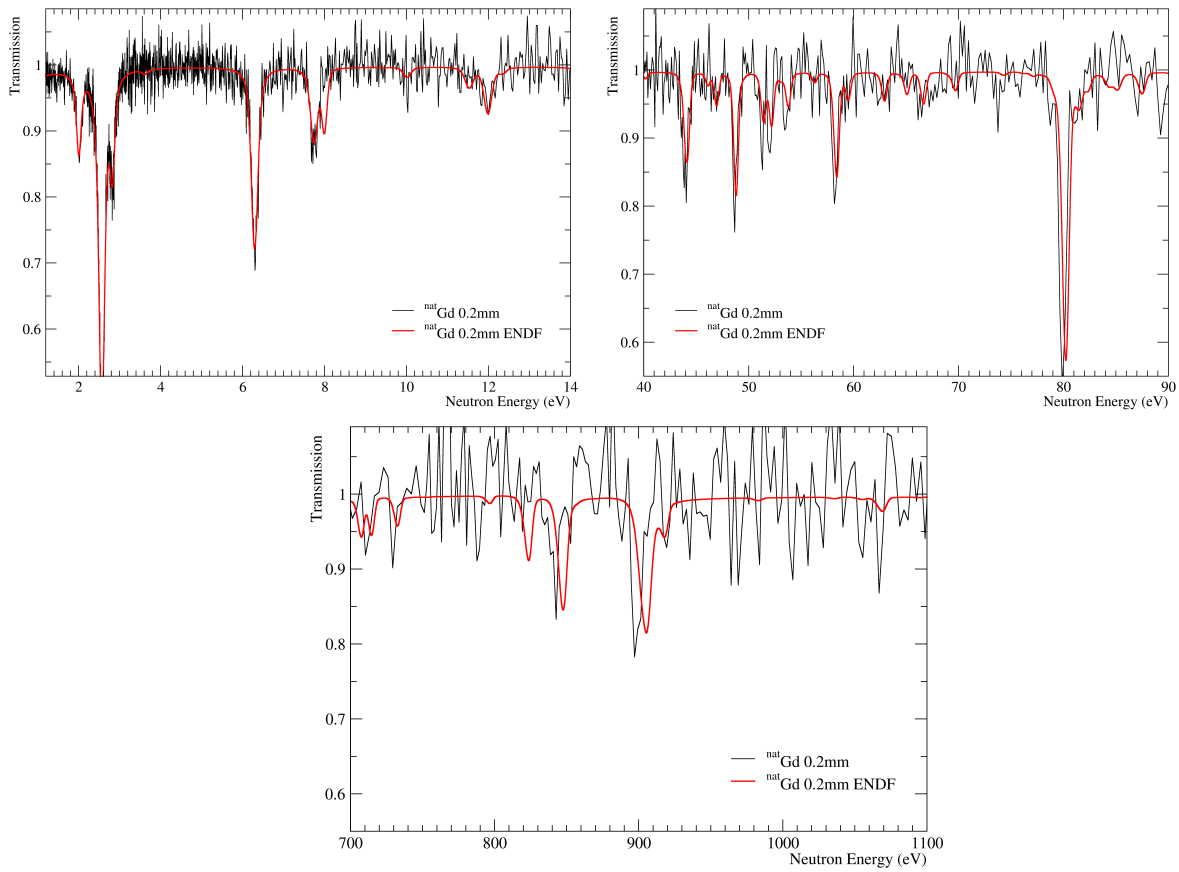

Figure 5.23: Magnification of three regions of the transmission spectrum obtained with the 0.2 mm ^{nat}Gd sample. Up left: energy region around the 8 eV resonance of ^{152}Gd, up right: energy region around the 65 eV resonance of ^{154}Gd, down: energy region around the 906 eV resonance of ^{160}Gd.

Isotope	Resonance energy (eV)
^{152}Gd	8.00
^{154}Gd	65.06
^{155}Gd	2.57, 6.30, 21.02
^{156}Gd	33.12, 80.20, 198.10
^{157}Gd	16.77, 20.56, 48.80
^{158}Gd	22.30, 409.10, 847.30
^{160}Gd	222.00, 478.90, 904.90

Table 5.5: List of gadolinium resonances suitable for isotopic characterization of enriched samples.

As we can see from the images, these three resonances, especially the ^{152}Gd and ^{154}Gd ones, are too small to be correctly analysed. In both cases, we have a transmission higher than 0.9 and both resonances are near to other isotopes resonances of similar width. In particular, the 8 eV and 65 eV are the only resonances that can be used for ^{152}Gd and ^{154}Gd respectively.

To perform a good isotopical characterization of the samples a new measurement with thicker natural gadolinium samples is necessary. This new measurement has to be performed with samples of at least 0.5 mm of thickness. In Fig.5.24 the calculated transmission for a 1 mm ^{nat}Gd sample is shown in the same energy region of Fig.5.23. As we can notice from this comparison, with a natural sample of 1 mm thickness the transmission obtained for the three resonances is below 0.85. Moreover, the ^{152}Gd resonance at 8 eV, although it is nearby the 7.7 eV resonance of ^{155}Gd, has a transmission below 0.6 and it is separated enough to be analysed. The 906 eV of ^{160}Gd has a transmission close to 0.4 and also the 848 eV resonance of ^{158}Gd could be fully analysed.

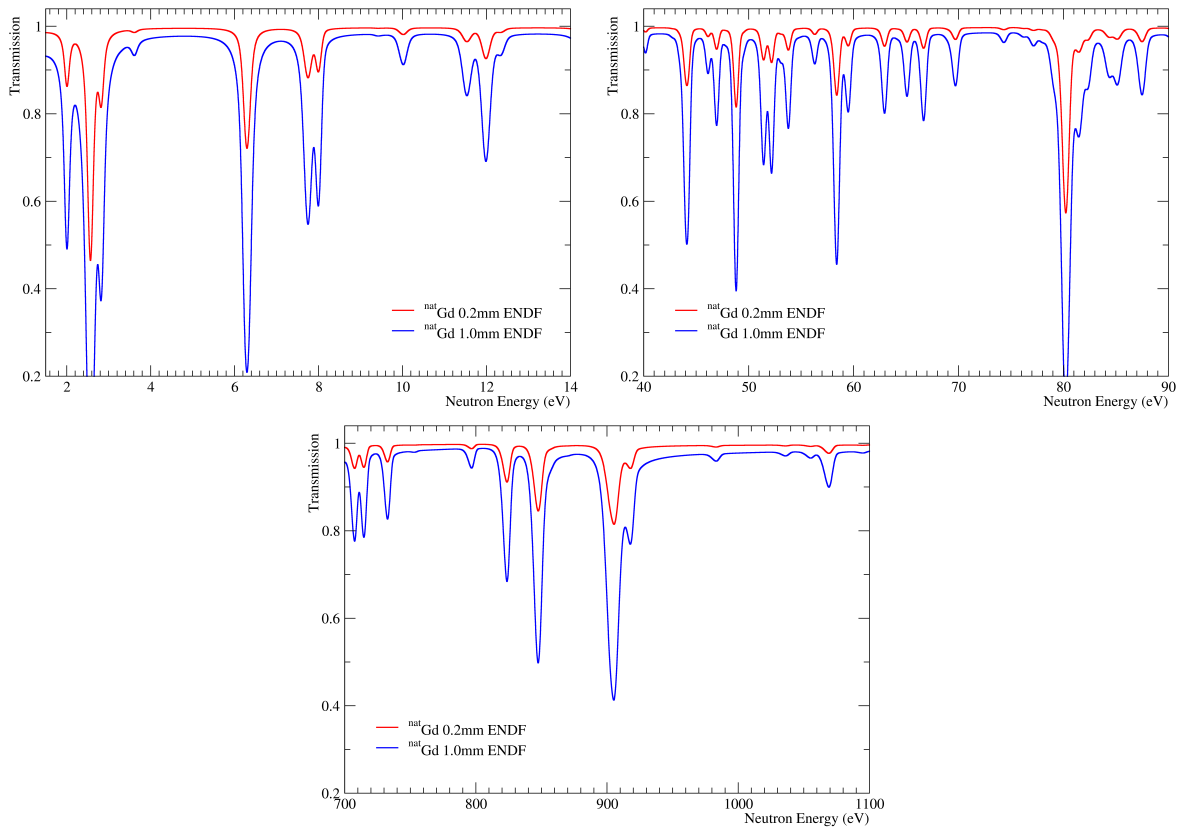

Figure 5.24: Magnification of three regions of the transmission calculated for 0.2 mm (red) and 1.0 mm (blue) ^{nat}Gd samples. Up left: energy region around the 8 eV resonance of ^{152}Gd, up right: energy region around the 65 eV resonance of ^{154}Gd, down: energy region around the 906 eV resonance of ^{160}Gd.

Conclusions

Gadolinium is a very important nuclide for many scientific fields ranging from nuclear energy to nuclear medicine and neutrino detection. This nuclide is so relevant because of its neutron thermal cross section, which is one of the biggest in nature. This cross section is caused mainly by its odd isotopes ^{155}Gd and ^{157}Gd. So far, there are many inconsistencies in the measurement of these cross sections in literature with differences up to 12%.

To improve the precision of the neutron thermal cross section of gadolinium odd isotopes a transmission measurement was performed at the EC-JRC of Geel on different enriched and natural gadolinium samples. The measurements were performed at the 10 m flight-path station of GELINA, the time-of-flight facility of JRC. The neutron beam was produced by the collision of an electron beam with a rotating uranium target. The samples used were five enriched (two ^{155}Gd, two ^{157}Gd and one ^{154}Gd) and four natural Mg 0.25% wt Gd alloys of different thicknesses. The transmission detector was a ^{6}Li glass scintillator. All the measurements were performed between May 2018 and June 2019.

In this work, all the analysis procedure, ranging from data reduction to the Resonance Shape Analysis, was described. The analysis concentrated in the thermal region, in particular in the region below 1 eV for the natural samples and the thin ^{155,157}Gd enriched samples and below 100 eV for the thicker samples. The first set of samples was used to obtain the parameters of the thermal resonances of ^{155,157}Gd and to obtain a new estimation of the thermal capture cross section of both isotopes. The natural gadolinium alloys offered a very important way to validate these parameters and to study in detail

the transmission of very thin natural gadolinium. The obtained cross sections are 59.7(3) kb and 244(2) kb for ^{155}Gd and ^{157}Gd respectively. Comparing these values with the ones obtained in the capture experiment performed at n_TOF using the same enriched samples [1] (62.2(2.2) kb and 239.8(8.4) kb respectively) we can notice a good agreement below 4% and compatibility within errors. Moreover, we can see how this new measurement of ^{157}Gd thermal cross section is not compatible with the Leinweber one [18](226 kb, 8% lower than our estimation) which is the measurement with the higher deviation from the value in libraries. Also, this new evaluation is 3% lower of the ENDF value (253.32 kb). The thermal cross section of ^{155}Gd is compatible with the ENDF library (60.89) within 2%.

These values of neutron cross section reproduce very well also the behaviour of natural gadolinium. We observed a deviation below 2σ between the data and the theoretical transmission calculated with the new parameters. The only exception to this behaviour is the low energy region of the 3.0 mm MgGd sample. In this sample, we observed a structure that cannot be reproduced. A further investigation of this sample will be carried out with a capture measurement at GELINA.

A Resonance Shape Analysis on some of the biggest resonances of ^{155,157}Gd was also performed using the data obtained with thicker samples. We analysed a total of seven and five resonances for ^{155}Gd and ^{157}Gd respectively. This analysis was performed only for resonances with a transmission below 0.9. For all the ^{155}Gd resonances we can see a difference of a few σ between our results and the n_TOF ones. For ^{157}Gd there is a big difference in capture width for the higher energy resonances. This difference cannot be explained and requires further investigations.

The ^{154}Gd enriched sample was used to test the ^{155}Gd contamination. Using three of the biggest resonances analysed, it was possible to obtain a value of 19.8% while the manufacturer declared contamination was 17.5%, a difference of 10%. To perform a complete characterization of all these samples an accurate measurement with a thick ^{nat}Gd sample is required. Analysing a transmission measured performed in 2015 at GELINA with thin ^{nat}Gd samples, we saw that a new measurement with a set of natural

gadolinium samples of at least 1 mm of thickness is necessary to perform a complete isotopic characterization of gadolinium samples.

In conclusion, all the results obtained in this experimental campaign are compatible with the ones obtained at n_TOF with the same set of samples. This compatibility with an experiment performed with different conditions (flight-path length, detection system, neutron production ecc.) validate the results obtained by both experiments. We believe that these new evaluations of gadolinium odd isotopes thermal cross section will help to reduce the uncertainty on these values.

Acknowledgements

This thesis is based on the measurements performed in collaboration with Dr. C.Paradela. A special thanks goes to P.Schillebeeckx and S.Kopecky for their valuable comments.

This work has been partially supported by the ENEN+ project that has received funding from the Euratom research and training Work Programme 2016 2017 1 #755576.

Bibliography

[1] M. Mastromarco et al., *Cross section measurements of* ^{155,157}*Gd(n,*γ*) induced by thermal and epithermal neutrons*, Eur. Phys. J. A **55**, 9 (2019).

[2] M.C.Moxon, *REFIT-2013, A Least Square Fitting Program for Resonance Analysis of Neutron Transmission, Capture, Fission and Scattering Data*, User manual (2013).

[3] https://ec.europa.eu/jrc/en/eufrat

[4] F. Rocchi et al., *Reassessment of gadolinium odd isotopes neutron cross sections: scientific motivations and sensitivity-uncertainty analysis on LWR fuel assembly criticality calculations*, EPJ Nuclear Sci. Technol. **3**,21 (2017).

[5] H. Grard, *Physique, fonctionnement et sûreté des REP*, EDP Sciences, Les Ulis (2014).

[6] http://www.cea.fr/english

[7] D. Bernard, A. Santamarina, *Qualification of gadolinium burnable poison: Interpretation of MELUSINE/GEDEON-II spent fuel analysis*, Ann. Nucl. Eng. **87**, 21 (2016).

[8] J.P.A. Renier, M.L Grossbeck, *Development of Improved Burnable Poisons for Commercial Nuclear Power Reactors*, Oak Ridge National Laboratory Report ORNL/TM-2001/238, (2001).

[9] French Law 1488, 2010: Nouvelle Organisation du March de lElectricit.

[10] D. Serghiuta, O. Nainer, *The Burnable Poisons Utilization for Fissile Enriched CANDU Fuel Bundle*, presented at 19^{th} CNS Nuclear Simulation Symposium, Hamilton (1995).

[11] K. Hagiwara et al., *Gamma Ray Spectrum from Thermal Neutron Capture on Gadolinium-157*, Prog. Theor. Exp. Phys. (2015).

[12] http://www-sk.icrr.u-tokyo.ac.jp/sk/index-e.html

[13] Sekiya, Hiroyuki, *The Super-Kamiokande Gadolinium Project*, PoS , **ICHEP2016**, 982 (2016).

[14] D. Alberti et al., *A theranostic approach based on the use of a dual boron/Gd agent to improve the efficacy of Boron Neutron Capture Therapy in the lung cancer treatment*, Nanomedicine: Nanotechnology, Biology and Medicine, **11**, 741 (2015).

[15] S.F.Mughabghab, *Atlas of Neutron Resonances*, Elsevier, Holland (2006).

[16] H.B. Moller et al., *Low energy neutron resonances in erbium and gadolinium*, Nucl. Sci. Eng, **8**, 183 (1960).

[17] S.F. Mughabghab et al., *Neutron cross sections, Resonance parameters*, Brookhaven National Laboratory Report BNL-325, third edition (1973).

[18] G. Leinweber et al., *Neutron capture and total cross section measurements and resonance parameters of gadolinium*, Nucl. Sci Eng. **154**, 261 (2006).

[19] Y.R. Kang et al., *Neutron capture measurements and resonance parameters of gadolinium*, Nulc. Sci. Eng. **180**, 86 (2015).

[20] B. Baramsai et al., *Neutron resonance parameters in ^{155}Gd measured with DANCE γ-ray calorimeter array*, Physical review C **85**,(2012).

[21] H.D. Choi et al., *Radiative capture cross sections of ^{155,157}Gd for thermal neutrons*, Nucl. Sci Eng. **177**, 219 (2014).

[22] Y. Ohno et al. *The total cross section of some rare-earth elements for 2200 m/sec neutrons*, Japanese report to EANDC **10**, 1 (1968).

[23] https://www-nds.iaea.org/exfor/

[24] F. Becvar, *Simulation of cascades in complex nuclei with emphasis on assessment of uncertainties of cascade-related quantities*, Nucl. Instrum. and Meth. A **417** 434 (1998).

[25] C.E. Porter and R.G. Thomas, *Fluctuations of Nuclear Reaction Width*, Phys. Rev **104**, 493 (1956).

[26] C. H. Westcott, *The specification of neutron flux and nuclear cross-sections in reator calculations*, Journal on Nuclear Energy **2** 59 (1954).

[27] P. Schillebeeckx et al, *Determination of Resonance Parameters and their Covariances from Neutron Induced Reaction Cross Section Data*, Nuclear Data Sheets **113** 3054 (2012).

[28] https://www.mitutoyo.co.jp/eng/

[29] W. Mondelaers and P. Schillebeeckx, *GELINA a neutron time-of-flight facility for high-resolution neutron data measurements*, Notiziario Neutroni e Luce di Sincrotrone **11**, 19 (2006).

[30] S. Kopecky and A. Brusgan, *The total neutron cross section of* ^{61}*Ni*, Nuclear Physics A **773**, 173 (2006).

[31] K. Berthold, C. Nazareth, G. Rohr and H. Weigmann, *Very high resolution measurements of the total cross section of natural Iron*, Proceedings of the international conference on nuclear data for science and technology, 218 (1994).

[32] S. Kopecky, P. Siegler and A. Moens, *Low energy transmission measurements of* ^{240,242}*Pu at GELINA and their impact on the capture width*, Proceedings of the in-

ternational conference on nuclear data for science and technology, 623 (1994) edited by O. Bersillon et al. (CEA, Paris, 2008).

[33] J. Heyse et al., *High Resolution Measurement of the ^{234}U(n,f) Cross Section in the Neutron Energy Range from 0.5 eV to 100 keV*, Nucl. Sci. Eng. **156**, 211 (2007).

[34] L. De Smet et al., *Investigation of the (n,p) and (n,α) reactions on ^{26}Al and ^{36}Cl and their astrophysical relevance*, Nucl. Phys A **758**, 80 (2005).

[35] L. C. Mihailescu et al., *High resolution measurement of neutron inelastic scattering and (n,2n) cross-sections for ^{209}Bi*, Nucl. Phys A **799**, 1 (2008).

[36] https://scionix.nl/

[37] C. Paradela et al., *Electronic setup for time-of-flight cross section measurements at GELINA*, JRC technical reports, unpublished.

[38] Y.K.Kim et al., *Results of time-of-flight transmission Measurements for ^{197}Au at a 50 m station of GELINA*, JRC Scientific and policy report (2013)

[39] H. Derrien et al, *Neutron resonance parameters of ^{238}U and the calculated cross section from Reich-Moore analysis of experimental data in the neutron energy range from 0 keV to 20 keV*, ORNL/TM-2005/241, Oak Ridge National Laboratory, Oak RIdge, Tenn (2005).

[40] M.S.Moore, *Rate dependence of counting losses in neutron time-of-flight measurements*, Nucl. Instr. Meth. **169** 245 (1980).

[41] R.G.Thomas and A.M.Lane, *R-Matrix Theory of Nuclear Reactions*, Rev. Mod. Phys **30** 257 (1958).